12-2013

A Novel Approach to Multiphysics Modeling of Heat and Mass Transfer in Porous Media

Seth Allen Pemberton
University of Tennessee - Knoxville, spember3@utk.edu

To the Graduate Council:

I am submitting herewith a thesis written by Seth Allen Pemberton entitled "A Novel Approach to Multiphysics Modeling of Heat and Mass Transfer in Porous Media." I have examined the final electronic copy of this thesis for form and content and recommend that it be accepted in partial fulfillment of the requirements for the degree of Master of Science, with a major in Mechanical Engineering.

Kivanc Ekici, Rao V. Arimilli, Major Professor

We have read this thesis and recommend its acceptance:

Jay I. Frankel

Accepted for the Council:
Carolyn R. Hodges

Vice Provost and Dean of the Graduate School

(Original signatures are on file with official student records.)

A Novel Approach to Multiphysics Modeling of Heat and Mass Transfer in Porous Media

A Thesis Presented for the
Master of Science
Degree
The University of Tennessee, Knoxville

Seth Allen Pemberton
December 2013

Dedication

I dedicate this work to our Lord Jesus Christ for He has shown me that “the thief must no longer steal. Instead, he must do honest work with his own hands, so that he has something to share with anyone in need”. Without the blessing of Christ I would not be where I am at today. “For from Him and through Him and to Him are all things. To Him be the glory forever.”

I also dedicate this work to my loving wife Ashley and parents Lynn and Keith. Without their loving support and sacrifices I would not have made it this far. Thank you all.

Acknowledgements

I would like to thank my graduate committee, Dr. Jay Frankel, Dr. Rao V. Arimilli, and Dr. Kivanc Ekici. I would especially like to thank my advisors Dr. Ekici and Dr. Arimilli for the attention and support you have given me over the past years. Thank you for being patient with me and always willing to do what is in my best interest.

Abstract

This thesis aims to investigate conjugate heat and mass transfer in porous media with an emphasis on textiles. Both hygroscopic materials, those that absorb water vapor, and non-hygroscopic materials are examined. A model was developed that utilizes COMSOL's equation-based partial differential equation (PDE) interface which allows the user to input any equation(s) to be solved. By the use of experimental and numerical data each part of the model, i.e. flow field, gas diffusion, convection and vapor absorption, is verified. The accuracy of the equation-based unsteady flow field is verified by modeling the flow over a circular cylinder and extracting the lift and pressure coefficients. Gaseous diffusion in a porous medium (PM) is shown to agree with volume averaging theory. Steady state convection and diffusion is modeled and reveals the importance of mass diffusion in PM as well as how changes in material permeability, due to water vapor absorption, affect heat and mass transfer. Water vapor absorption yields a dynamic response under transient conditions, which results in significant temperature changes depending on textile fiber properties.

Table of Contents

List of Tables

List of Figures

Nomenclature

a	absorption coefficient in coefficient form PDE
c	diffusion coefficient in coefficient form PDE
c_p	apparent specific heat (at constant pressure) of all phases in porous medium (J/kgK)
$c_{p,a}$	specific heat (at constant pressure) of dry air (1007 J/kgK)
$c_{p,g}$	specific heat (at constant pressure) of mixture (J/kgK)
$c_{p,s}$	specific heat (at constant pressure) of solid matrix (J/kgK)
$c_{p,v}$	specific heat (at constant pressure) of water vapor (1872 J/kgK)
$c_{p,w}$	specific heat (at constant pressure) of liquid water (4179 J/kgK)
C	species concentrations (mol/m^3)
d_a	time derivative coefficient
d_f	effective fiber diameter (m)
D	diameter (m)
D_{eff}	effective diffusion coefficient in porous medium (m^2/s)
D_s	diffusion coefficient of water vapor to solid (m^2/s)
D_{va}	binary diffusion coefficient for air and water vapor (m^2/s)
e_a	second order time derivative coefficient
f	source term or vortex shedding frequency
k	absorption energy parameter
k_a	thermal conductivity for dry air (0.0263 W/mK)
k_{ds}	thermal conductivity of dry solid (W/mK)
k_{eff}	effective thermal conductivity of mixture and porous medium (W/mK)
k_g	thermal conductivity of gaseous phase (W/mK)
k_s	thermal conductivity of solid phase (W/mK)
k_v	thermal conductivity of water vapor (0.0196 W/mK)
k_w	thermal conductivity of liquid water (0.613 W/mK)
$\boldsymbol{I}$	identity matrix
L	heat of vaporization (J/kg)
m	number of absorption layers at the secondary sites
m_a	mass of dry air (kg)
$\boldsymbol{m}_{d,a}$	diffusive mass flux of dry air (kg/m^{2}s)
$\boldsymbol{m}_{d,v}$	diffusive mass flux of water vapor (kg/m^{2}s)
m_v	mass of water vapor (kg)
$\dot{m}$	volume-average mass flux of vapor to fiber (kg/m^{3}s)
M_a	molecular mass of dry air (28.97 g/mol)
M_v	molecular mass of water vapor (18.015 g/mol)
n	number of absorption layers at the primary sites
p	gauge pressure in flow field (Pa)
p_a	partial pressure of dry air (Pa)

p_{bottom}	average pressure on the bottom of porous medium (Pa)
p_{top}	average pressure on the top of porous medium (Pa)
p_v	partial pressure of water vapor (Pa)
$p_{v,sat}$	saturation vapor pressure of water vapor (Pa)
$\boldsymbol{q}$	diffusive heat flux (W/m^2)
$\boldsymbol{q}_g$	total diffusive heat flux of mixture (W/m^2)
Q	heat of adsorption (J/kg)
r	flow resistance (1/m)
r_{dry}	flow resistance when $\phi = 0.0$ (1/m)
r_{sat}	flow resistance when $\phi = 1.0$ (1/m)
R	universal gas constant (8.314 J/molK)
Re	Reynolds number
Re_D	Reynolds number based on diameter
R_a	specific gas constant for dry air (286.987 J/kgK)
R_{eq}	equilibrium regain at fiber surface
R_{sat}	regain of material when $\phi = 1.0$
R_v	specific gas constant for water vapor (461.504 J/kgK)
R_t	regain of the fiber at time t
R_0	regain for monolayer coverage
St	Strouhal number
t	time (s)
T	temperature (K)
$\boldsymbol{u}_g$	velocity of mixture (m/s)
U	freestream velocity (m/s)
V_g	total volume of mixture (m^3)
x_a	mass fraction of dry air
x_v	mass fraction of water vapor

Greek Symbols

α	fraction of absorption sites that may have up to n layers and conservative flux convection coefficient
β	convection coefficient
γ	conservative flux coefficient
ε	porosity
ε_{bw}	volume fraction of the water absorbed in solid
$\varepsilon_{bw,sat}$	volume fraction of the water absorbed in solid when $\phi = 1.0$
ε_g	volume fraction of the gaseous phase
θ_s	volume fraction of dry solid (constant)
κ	intrinsic permeability of porous medium (m^2)
μ	dynamic viscosity of air (1.846e^{-5} Pa s)

ρ	apparent density of all phases of porous medium (kg/m^3)
ρ_a	density of dry air (kg/m^3)
ρ_g	density of moist air mixture (kg/m^3)
ρ_s	density of solid matrix (kg/m^3)
ρ_v	density of water vapor (kg/m^3)
ρ_w	density of liquid water (1000 kg/m^3)
ϕ	relative humidity
φ	weak form test function
τ	tortuosity factor of porous medium

Subscripts

a	dry air
bw	bound water
d	diffusive component
ds	dry solid
eff	effective
g	gaseous phase
l	liquid
s	solid phases
sat	saturation
v	water vapor
w	water

Superscripts

T	transpose

Abbreviations

BC	boundary condition
CV	control volume
DOF	degree of freedom
PDE	partial differential equation
PM	porous medium

Chapter 1

Introduction

Porous media have been a subject of research for many years with applications to building materials, food processes, soil hydration and textiles. Of general interest in all of these areas is heat and mass transfer to and from the medium. Heat and mass transfer in itself can be challenging with the coupled nature of the two, but adding a porous medium with its complex structure only complicates the problem further. Porous media provide a resistance to heat and mass transfer which, depending on the application, can be desirable or undesirable. For example, in textiles if the climate is "cold" a person would wish to insulate himself/herself. On the contrary, if the climate is "hot" then the person desires to liberate heat and moisture as much as possible. The natural question to ask is, "what properties of the material deliver the above requirements?". Therefore, this work is directed towards a better understanding of the aspects or properties of porous media, through a general and novel computational model that considers heat and mass transfer. Of particular interest is the application of the developed technique to textile materials.

In many situations it is possible to have a liquid phase present inside the porous medium. For food processes, a liquid saturation is generally the case and thus the liquid phase is imperative to model. Building materials can certainly have a liquid phase due to rain or condensation, but most building materials are subject to water vapor changes and thus a liquid phase is not imperative to model. Similarly, textiles can exhibit a liquid

phase in the form of sweat (when clothing is the subject) and many researchers desire to model the evaporative drying in textiles. Such a case is not considered in this thesis since the majority of textiles are not subject to sweat but rather moist air from the surroundings and moisture leaving the body. For this work, only mild temperature gradients and conditions will be considered and it will be assumed that a liquid state is not present.

The model makes use of conjugate modeling to aid in the understanding of heat and mass transfer in porous media, eliminating the need to explicitly specify heat and mass transfer coefficients. Without conjugate modeling, experiments would have to be performed to determine these transfer coefficients for a specific medium and geometry. Additionally, the transfer coefficients would have a constant value over the entire surface and would not account for spatial and temporal differences. In contrast, conjugate modeling results in a more general model, and can further aid in the accuracy of more complex geometries. In terms of textiles, this could result in the modeling of the human body as the geometry. The general model permits one to use the intrinsic properties of a porous medium, such as porosity and permeability.

To incorporate conjugate modeling and all the desired physics with a complete control over the coupling of the multiphysics phenomena, equation-based modeling in COMSOL is used. To the best of the author's knowledge, equation-based modeling of this type of problem (multiphysics modeling of porous media) has not been done for fabrics before. For this reason, individual aspects of the model need to be verified just

to show that the governing equations themselves have been implemented correctly. Following this, the model also needs to be verified to determine if proper coupling of the physics has been achieved. Only through successful validation of the model can the simulations help understand the behavior of porous media that affect heat and mass transfer.

The thesis is structured as follows. In chapter 2, a literature review of work done in heat and mass transfer in porous media is detailed. The assumptions used and resulting governing equations are discussed in chapter 3. Chapter 4 presents the implementation of the governing equations into the equation-based approach. Steady-state and time dependent cases are presented in chapter 5 with conclusions in chapter 6.

Chapter 2

Literature Review

In the literature to date, many researchers have studied heat and mass transfer in porous media with a more recent emphasis on convective drying. Although drying is not considered in this work, the drying process involves the coupling of heat and mass transfer, which is one of the main objectives of this thesis. Rogers & Kaviany 1991 and Prommas 2011 studied convective drying of packed beds through numerical modeling and experiments. They showed that capillary action and particle size play an important role in drying and that two drying phases are present. De Bonis & Ruocco 2008 used a finite element model (COMSOL) to study drying of food with an Arrhenius-type evaporative kinetics. They made use of COMSOL's conjugate heat and mass transfer modules thereby eliminating the need to know heat transfer coefficients a priori. Masmoudi & Prat 1991, Defraeye, Blocken, and Carmeliet 2012, and Defraeye et al. 2012 investigated convective drying of unsaturated porous plates with the aim of comparing conjugate heat transfer modeling and constant heat transfer coefficient modeling. They reported that conjugate modeling results in a true two dimensional problem due to the spatial variation of the transfer coefficients as well as temporal variation from the material surface drying. This approach provides a more accurate model than a constant heat transfer approach and can give better results for more complex geometries or systems. The downside of this approach is that during certain drying periods of porous media, additional modeling effort is required. In spite of this

added effort, significantly more accurate results may not be obtained since the transfer rates depend on the porous medium properties rather than the external flow. Gibson & Charmchi 1997(2) investigated modeling of convective heat and mass transfer of hygroscopic fabrics and compared their results to experimental data. The main question they tried to answer was “how do the material fibers swell causing a decrease in porosity with an increase in relative humidity?”. Using a relation between relative humidity and material permeability, they were able to more accurately model convective heat and mass transfer through the fabric. Gibson & Charmchi 1997(1) also presented a model for one dimensional diffusive heat and mass transfer in textile fibrous materials with a human thermal model to provide boundary conditions. Hygroscopic and non-hygroscopic fabrics were investigated (as well as multilayered fabrics) revealing that hygroscopic materials have a dynamic response due to vapor absorption. Fan et al. 2000, 2004, Li & Zhu 2003, Canuto & Cimolin 2011, Zhang et al. 2011, and Hang et al. 2012 all presented models for heat and mass transfer taking into consideration phase change and vapor absorption. In all these works, vapor absorption was modeled as diffusion in and out of the solid structure of the medium. It must be noted that all of these models use the Hertz-Knudsen equation, or a variation thereof, to model evaporation/condensation in the material. In another work, Le & Ly 1992 modified well-known semi-empirical sorption relations for better agreement with experimental data. Using the improved sorption relation, Le et al. 1995 investigated steaming of fabrics with emphasis on the absorption physics.

In the following chapter we present the components of the moist air mixture and the physics involved in the model. Pertinent assumptions are made about both the mixture and porous medium, which *lead to the eleven governing equations* used for this problem. Conservation equations for mass, momentum and energy are discussed as well as the volume averaged properties for each component in the domain.

Chapter 3

Theory and Equations

Concepts of Fluid Flow

Moist Air

Moist air (subscript g) is modeled as a perfect mixture of two ideal gasses, namely dry air (subscript a) and water vapor (subscript v). For each component the ideal gas law can be defined:

$$p_a = \rho_a R_a T = \frac{m_a}{V_g} R_a T = x_a \rho_g R_a T \tag{1}$$

$$p_v = \rho_v R_v T = \frac{m_v}{V_g} R_v T = x_v \rho_g R_v T \tag{2}$$

where p_a and p_v are partial pressures, R_a and R_v are the specific gas constants, ρ_a and ρ_v are the densities, m_a and m_v are the masses and x_a and x_v are the mass fractions of dry air and water vapor, respectively. In addition, V_g is the mixture volume, ρ_g is the mixture density and T is the temperature. It is assumed that all mixture components are in thermal equilibrium and thus $T_a = T_v = T_g = T$. The mass fractions are related to each other through:

$$x_a + x_v = 1 \tag{3}$$

whereas densities for each component are related to the mass fractions by

$$\rho_a = x_a \rho_g \tag{4}$$

$$\rho_v = x_v \rho_g \tag{5}$$

Using equations (3)-(5), the density of the mixture can be written as

$$\rho_g = \rho_a + \rho_v \tag{6}$$

The specific gas constants are determined from the universal gas constant R (8.314 J/molK) and the molecular weight of air M_a (28.97 g/mol) and water vapor M_v (18.015 g/mol) through

$$R_a = \frac{R}{M_a} \qquad R_v = \frac{R}{M_v} \tag{7}$$

To quantify the amount of moisture in the air, relative humidity (ϕ) is introduced, which is expressed by

$$\phi = \frac{p_v}{p_{v,sat}} \tag{8}$$

where $p_{v,sat}$ is the saturation pressure of the vapor. Note that $p_{v,sat}$ is a function of temperature and is given by (Gibson & Charmchi 1997(2))

$$p_{v,sat} = 614.3exp\left\{17.06\left[\frac{(T-273.15)}{(T-40.25)}\right]\right\} \tag{9}$$

Gas Diffusion

Fick's law governs the diffusive mass flux, which specifies the concentration gradient as the driving force. For binary mixtures, such as moist air, the vapor diffusive fluxes are denoted by $\boldsymbol{m}_d$ and are expanded as

$$\boldsymbol{m}_{d,a} = -\rho_g D_{va} \boldsymbol{\nabla} \frac{\rho_a}{\rho_g} \tag{10}$$

$$\boldsymbol{m}_{d,v} = -\rho_g D_{va} \boldsymbol{\nabla} \frac{\rho_v}{\rho_g} \tag{11}$$

where D_{va} is the binary diffusion coefficient for water vapor and air. D_{va} is dependent on temperature through the follow equation (Gibson & Charmchi 1997(2))

$$D_{va} = 2.23x10^{-5}\left(\frac{T}{273.15}\right)^{1.75} \quad (12)$$

Temperature gradients can also induce mass diffusion by the thermo-diffusion effect. This effect will be neglected in this thesis since such high temperature gradients are not considered.

Heat Conduction

Heat conduction, or the diffusive heat flux, is governed by Fourier's law where the driving force is temperature gradient which is given by

$$\boldsymbol{q} = -k_g \boldsymbol{\nabla} T \quad (13)$$

where k_g is the thermal conductivity of the gaseous phase. This conductivity is moisture dependent but has small variability since the mixture (moist air) is assumed to be dilute. When a mixture is considered, there is an additional contribution to the heat flux due to the diffusion of the different mixture components (Bird et al. 2002, Defraeye 2011). This is given by

$$\boldsymbol{q}_g = \boldsymbol{q} + \sum_i c_{p,i} \boldsymbol{m}_{d,i} T \quad (14)$$

where $\boldsymbol{q}_g$ is the total heat flux of the mixture and $\boldsymbol{m}_{d,i}$ is the diffusive mass flux of a component. Ultimately, the summation term above will become part of the convection coefficient as will be described later.

External Flow

Since this work aims to investigate convective heat and mass transfer to (and from) a porous medium (PM), there is flow external to the PM. Therefore, one must consider conservation of mass, momentum, and energy. In order to present the conservation equations for the external flow field, the assumptions made in this work need to be stated. Below are the assumptions taken into account and the resulting conservation equations.

Assumptions

1. Moist air is a perfect mixture of ideal gases: dry air and water vapor and is a Newtonian fluid.
2. Properties (and the fluid) are assumed isotropic.
3. Moist air is assumed incompressible although the mixture density varies with humidity.
4. Water is assumed to be in only one phase in the air, namely water vapor.
5. No mass or heat sources are taken into account.
6. Momentum source terms are not taken into account.
7. Thermal equilibrium is assumed between all mixture components.
8. Potential energy changes (gravity) are assumed to be small compared to thermal energy changes and are neglected.
9. Pressure work is neglected.
10. Viscous heat/dissipation is neglected.

Conservation of Mass

In this work, dry air and water vapor are both accounted for in the external flow. The basic conservation of mass principle states that: the rate of increase of mass in a control volume (CV) plus the mass transported by the flow is equal to the rate of transfer by diffusion, sources and sinks. Since there are no sources or sinks in the external flow the resulting equations for dry air and water vapor are

$$\frac{\partial \rho_a}{\partial t} + \boldsymbol{\nabla} \cdot \left(-D_{va} \rho_g \boldsymbol{\nabla} \frac{\rho_a}{\rho_g} \right) + \boldsymbol{u}_g \cdot \boldsymbol{\nabla} \rho_a = 0 \tag{15}$$

$$\frac{\partial \rho_v}{\partial t} + \boldsymbol{\nabla} \cdot \left(-D_{va} \rho_g \boldsymbol{\nabla} \frac{\rho_v}{\rho_g} \right) + \boldsymbol{u}_g \cdot \boldsymbol{\nabla} \rho_v = 0 \tag{16}$$

where ρ_i is the density of component i, D_{va} is the binary diffusion coefficient for water vapor and air, $\boldsymbol{u}_g$ is the gas mixture velocity, and subscripts a, v and g denote air, water vapor, and gas mixture, respectively.

Conservation of Momentum

Proceeding similarly to conservation of mass, conservation of momentum states that: the rate of change of momentum in a CV plus the momentum transported by the flow is equal to the rate of transfer of momentum by molecular transport and external forces. Neglecting body forces acting on the fluid, the momentum and continuity equations can be written as

$$\rho_g \frac{\partial \boldsymbol{u}_g}{\partial t} + \rho_g (\boldsymbol{u}_g \cdot \boldsymbol{\nabla}) \boldsymbol{u}_g = -\boldsymbol{\nabla} p + \mu \nabla^2 \boldsymbol{u}_g \tag{17}$$

$$\frac{\partial \rho_g}{\partial t} + \boldsymbol{\nabla} \cdot \left(\rho_g \boldsymbol{u}_g\right) = 0$$

for the external flow domain.

Conservation of Energy

Finally, conservation of energy states that: the rate of change of the total internal energy in a CV plus the internal energy transported by the flow is equal to the rate of heat transfer by conduction, mass diffusion, work done by surface and body forces and the contribution of sources or sinks. Neglecting sources and viscous heating and dissipation the resulting energy equation is given by

$$\begin{aligned}\left(\rho_a c_{p,a} + \rho_v c_{p,v}\right)\frac{\partial T}{\partial t} \\ + \left[c_{p,a}\left(\rho_a \boldsymbol{u}_g - D_{va}\rho_g \boldsymbol{\nabla}\frac{\rho_a}{\rho_g}\right)\right. \\ \left. + c_{p,v}\left(\rho_v \boldsymbol{u}_g - D_{va}\rho_g \boldsymbol{\nabla}\frac{\rho_v}{\rho_g}\right)\right] \cdot \boldsymbol{\nabla} T = \boldsymbol{\nabla} \cdot \left(k_{eff} \boldsymbol{\nabla} T\right)\end{aligned} \tag{18}$$

where

$$k_{eff} = \frac{\rho_a k_a + \rho_v k_v}{\rho_a + \rho_v} \tag{19}$$

and $c_{p,i}$ is the specific heat of component i, k_i is the thermal conductivity of component i, and T is the temperature. It can be seen that the effective thermal conductivity k_{eff} is based on the mass fraction of each component of the gas mixture.

Porous Medium

In general, porous materials consist of three different phases: (1) the solid phase (subscript *s*), which accounts for the solid matrix of the porous material such as fibers of a fabric; (2) the liquid phase (subscript *l*), or liquid water; and (3) the gaseous phase (subscript *g*), namely moist air. Here, the gaseous phase is considered to be a perfect mixture of two ideal gases as in the external flow. Also, the water vapor has the ability to penetrate into the solid porous matrix in the case of hygroscopic materials like cotton. Such physics are considered in this thesis and will be referred to as bound water and denoted by subscript *bw*.

Porous media can be analyzed in a number of ways, three of which are listed. (1) The microscopic scale, which differentiates between the micro-pores and grains for each material component; (2) the mesoscopic scale where each material component is viewed as homogeneous but is clearly distinguished from each other; and (3) the macroscopic scale where components are no longer differentiated and the material appears homogeneous. In this thesis the macroscopic scale is used with a continuum approach.

All porous materials are assumed to have a porosity, ε, which is defined as the ratio of the volume of the pores, V_{pore}, to the total volume of the PM, V. Therefore,

$$\varepsilon = \frac{V_{pore}}{V} \tag{20}$$

The dry solid matrix is defined as

$$\theta_s = 1 - \varepsilon \tag{21}$$

Since water vapor can be absorbed into the material, this results in a volume change of the material. This volume change will be constrained to just the fibers of the material and not the total volume of the PM. Thus the total volume of the PM will not change, instead the absorbed water will result in the swelling of the fibers, which in turn reduces the porosity. Therefore, the bound water will have a volume fraction (ε_{bw}) and the following constraint can be imposed

$$\varepsilon_g + \varepsilon_{bw} + \theta_s = 1 \tag{22}$$

It can be seen that, as the fibers swell the volume fraction of the gaseous phase will decrease.

Assumptions

1. There are two phases considered, namely solid and gaseous, where the solid phase consists of the solid porous matrix, and air/water vapor mixture makes up the gaseous phase. When the water vapor is absorbed by the solid matrix it is then considered part of the solid.
2. Moist air is a perfect mixture of ideal gases: dry air and water vapor.
3. Moist air and the solid material are assumed incompressible.
4. The solid matrix does not move.
5. The only heat and mass source terms are due to vapor absorption/desorption.

6. Potential energy changes are assumed to be small compared to thermal energy changes and are neglected.
7. Pressure work is neglected.
8. Viscous heating/dissipation is neglected.

Porous Medium Conservation of Mass

Diffusion

Within the PM there is convection and diffusion of dry air and water vapor. The diffusive flux in the PM is modeled using Fick's Law, which is given for a binary mixture as part the conservation of mass in the external flow. For diffusion in a PM the binary diffusion coefficient becomes the effective (or apparent) diffusion coefficient. Such factors as tortuosity (τ) of the material pores, liquid saturation, and porosity influence the rate of diffusion and result in an effective diffusion coefficient defined by

$$D_{eff} = \frac{D_{va}\varepsilon_g}{\tau} \tag{23}$$

Equation (23) can be viewed as a semi-empirical equation. From volume averaging, the effective diffusion coefficient has a more rigorous definition which is where the multiplication by the porosity comes from, but it also incorporates the dispersion tensor (Whitaker 1977). Dispersion is not addressed explicitly in this work. Alternatively, what is commonly done to account for dispersion and molecule-pore interaction, is to multiple by a scalar, which is called the tortuosity. Tortuosity is then determined through experiments.

Bound Water

When water vapor comes in contact with a fiber it can adsorb to the surface. In general there are two stages to adsorption. The first stage is when the vapor molecules cover the surface of the material and the second stage is when additional molecules stack on top of the first layer. Once the molecules cover the surface they can begin to permeate into the fiber. The resulting change in moisture content of the fiber is associated with the liberation or absorption of the heat of sorption. Thus, accounting for moisture absorption not only affects the fiber structure but also the total energy of the process.

In order to determine the amount of moisture absorbed by the fibers, the sorption isotherm is needed. The sorption isotherm, measured in terms of the mass of moisture to mass of solid, or regain, describes the equilibrium moisture content of a material at a given temperature. Le & Ly 1992 developed a semi-empirical equation for sorption isotherms based on four parameters. The parameters are found by curve fitting experimental data. The equation for the moisture absorption, or regain, as a function of relative humidity ϕ is given by Le & Ly 1992 as

$$R_{eq} = R_0 \frac{k\phi}{1+k\phi}\left[\frac{1-\alpha\phi^n-(1-\alpha)\phi^m}{1-\phi}\right] \tag{24}$$

where R_{eq} is the equilibrium regain, R_0 is the regain in the fiber for monolayer coverage, α is the fraction of the surface with n layers while remaining parts of the surface will have up to m layers. Finally, parameter k is related to the adsorption energy exponentially through

$$k = e^{\frac{QM}{RT}} \tag{25}$$

where Q is the heat of adsorption, M is the molecular weight and R is the universal gas constant. Figure 1 shows a representative curve for regain as a function of humidity.

It is assumed that the diffusion into the fiber is a quasi-steady state process (Le & Ly 1992). Also, it is assumed that the fiber surface immediately comes into equilibrium with the surrounding humidity. This equilibrium is characterized by the equilibrium regain given by equation (24). Suppose a dry porous material is suddenly exposed to moist air. When the moisture comes in contact with the dry fibers, the surface of the fiber will instantaneously have a regain equivalent to R_{eq} while the inside of the fiber has zero moisture content. Therefore, there is a moisture potential present from the outside of the fiber to the inside or vice versa. With this potential, the mass flow in and out of the fiber can be calculated as a difference in regains as (Le & Ly 1992)

$$\dot{m} = \frac{D_s \rho_s}{d_f^2}\left(R_{eq} - R_t\right) \tag{26}$$

where D_s is the diffusion coefficient for water vapor and the solid fiber, ρ_s is the solid matrix density, d_f is the fiber diameter, and the regain inside the fiber at time t is

$$R_t = \frac{\rho_w \varepsilon_{bw}}{\rho_s} \tag{27}$$

The resulting continuity equation for the bound water is then given as (Gibson & Charmchi 1997(2))

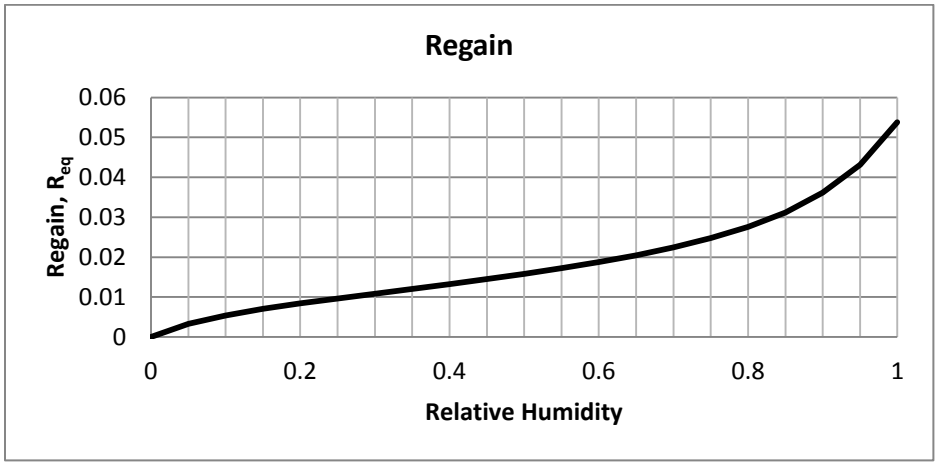

Figure 1. Representative regain curve

$$\rho_w \frac{\partial \varepsilon_{bw}}{\partial t} + \dot{m} = \rho_w \frac{\partial \varepsilon_{bw}}{\partial t} + \frac{D_s \rho_s}{d_f^2}\left(R_{eq} - \frac{\rho_w \varepsilon_{bw}}{\rho_s}\right) = 0 \tag{28}$$

Putting the above physics together and noting that the constraint on volume fraction is $\varepsilon_g + \varepsilon_{bw} + \theta_s = 1$, we get

$$\frac{\partial}{\partial t}\left(\varepsilon_g \rho_i\right) = \varepsilon_g \frac{\partial \rho_i}{\partial t} - \rho_i \frac{\partial \varepsilon_{bw}}{\partial t} \tag{29}$$

for any gas component i. This leads to conservation of mass for the entire system given by

$$\begin{gathered} \rho_w \frac{\partial \varepsilon_{bw}}{\partial t} + \dot{m} = 0 \\ \varepsilon_g \frac{\partial \rho_a}{\partial t} + \boldsymbol{\nabla} \cdot \left(-D_{eff} \rho_g \boldsymbol{\nabla} \frac{\rho_a}{\rho_g}\right) + \boldsymbol{u}_g \cdot \boldsymbol{\nabla} \rho_a - \rho_a \frac{\partial \varepsilon_{bw}}{\partial t} = 0 \\ \varepsilon_g \frac{\partial \rho_v}{\partial t} + \boldsymbol{\nabla} \cdot \left(-D_{eff} \rho_g \boldsymbol{\nabla} \frac{\rho_v}{\rho_g}\right) + \boldsymbol{u}_g \cdot \boldsymbol{\nabla} \rho_v - \rho_v \frac{\partial \varepsilon_{bw}}{\partial t} = -\dot{m} \end{gathered} \tag{30}$$

Porous Medium Conservation of Momentum

To determine the velocity field, the "Brinkman extension of Darcy's law" (Nield & Bejan 1999) was chosen since the same velocity and pressure fields are solved for both inside and outside the PM. Also since the PM is thin with high porosity (for textiles) and a no-slip condition needs to be specified, this equation is appropriate (Nield & Bejan 1999). Therefore, the resulting momentum equation for a PM becomes

$$\frac{\rho_g}{\varepsilon_g}\left(\frac{\partial \boldsymbol{u}_g}{\partial t}+\left(\boldsymbol{u}_g\cdot\boldsymbol{\nabla}\right)\frac{\boldsymbol{u}_g}{\varepsilon_g}\right)$$

$$=-\boldsymbol{\nabla}p+\boldsymbol{\nabla}\cdot\left\{\frac{1}{\varepsilon_g}\left[\mu\left(\boldsymbol{\nabla}\boldsymbol{u}_g+\left(\boldsymbol{\nabla}\boldsymbol{u}_g\right)^T\right)-\frac{2}{3}\mu(\boldsymbol{\nabla}\cdot\boldsymbol{u}_g)\boldsymbol{I}\right]\right\}-\frac{\mu}{\kappa}\boldsymbol{u}_g \qquad (31)$$

$$\frac{\partial \rho_g}{\partial t}+\boldsymbol{\nabla}\cdot\left(\rho_g\boldsymbol{u}_g\right)=0$$

where $\kappa=\kappa(\phi)$ is the humidity dependent permeability of the PM and $\boldsymbol{I}$ is the identity matrix.

Permeability

One of the important parameters in any porous media convective transport problem is the permeability of the material. Changes in the permeability result in velocity magnitude changes within the PM. As mentioned earlier, in the presence of humidity, a hygroscopic fabric will absorb the water vapor and fiber swelling will occur, which tends to close off the pores resulting in convective flow resistance. Therefore, heat and mass transfer will be affected by the change in the fiber structure. Such changes in convective flow properties have been studied by Wehner et al. 1987 who

showed that large changes to flow properties can occur in woven and nonwoven textiles due to fiber swelling. Similarly, Gibson & Charmchi 1997(2) have shown the same through experiments where an apparent flow resistance was measured against humidity for different fabrics. As an example, Figure 2 is a plot of the results of Gibson & Charmchi 1997(2) for flow resistance as a function of relative humidity. Hygroscopic materials such as cotton, wool, and silk show a higher resistance at high humidity whereas less hygroscopic materials like polyester show nearly no change in flow resistance. Accordingly, Gibson & Charmchi 1997(2) made the observation that the flow resistance follows a similar shape as a fabric sorption relation and thus the sorption relation can be used to approximate the permeability as the humidity changes.

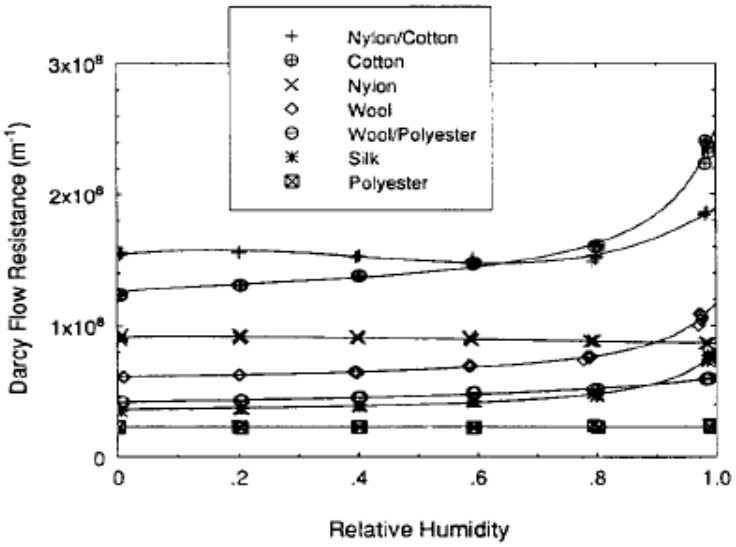

Figure 2. Flow resistance data of Gibson & Charmchi 1997(2)

Although the flow field in the PM is not modeled with Darcy's law but rather an extension of it, it will be assumed that the Darcy permeability and the permeability given in equation (31) are the same. With that assumption, from Darcy's law, which is given as

$$u = \frac{-\kappa}{\mu}\frac{\Delta p}{\Delta x} \tag{32}$$

the apparent resistance can be defined as

$$r = \frac{\Delta p}{\mu u} \tag{33}$$

Therefore, the permeability can be determined from the apparent resistance as

$$\kappa = \frac{\Delta x}{r} \tag{34}$$

With the sorption relation for a given material, the following approximation can be made to find the humidity dependent permeability:

$$r(\phi) = r_{dry} + \left(\frac{\varepsilon_{bw}(\phi)}{\varepsilon_{bw,sat}}\right)\left(r_{sat} - r_{dry}\right) \tag{35}$$

where r_{dry} is the resistance when $\phi = 0$, r_{sat} is the resistance when $\phi = 1.0$ and $\varepsilon_{bw,sat}$ is the volume fraction of bound water when $\phi = 1.0$. From the experiments of Gibson & Charmchi 1997(2), transport properties for seven fabrics were determined and are presented in Table 1. Figure 3 shows the humidity dependent permeability for the properties of cotton from Table 1. The shape of the curve will be the same for each hygroscopic material.

Table 1. Diffusive Transport Properties

Material	Diffusive Properties		Flow Resistance	
	D_{eff} Fabric Diffusivity $[m^2/s] \times 10^{-6}$	τ Tortuosity Factor	$r_{dry}(\phi = 0)$ $[m^{-1}] \times 10^8$	$r_{sat}(\phi = 1.0)$ $[m^{-1}] \times 10^8$
Wool	6.63	2.35	0.614	1.080
Silk	4.09	3.94	0.353	0.760
Cotton	7.60	2.12	1.230	2.400
Wool/Polyester	7.24	2.14	0.425	0.595
Nylon/Cotton	5.97	2.49	1.500	1.850
Nylon	8.87	1.82	0.930	0.868
Polyester	11.9	1.5	0.226	0.226

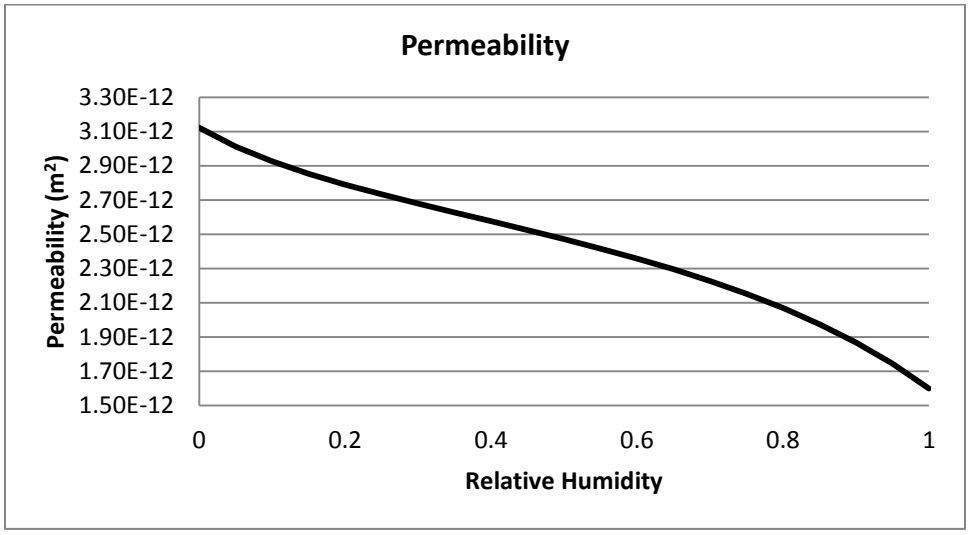

Figure 3. Humidity dependent permeability

Porous Medium Conservation of Energy

We saw that in the external flow, the mixture properties were based on the mass fractions of each component. Similarly, the properties of the PM are based on volume

fractions. First, consider the solid phase. When the water vapor is absorbed into the dry solid matrix, it is assumed to become immobile and part of the solid matrix. Therefore, the effective thermal conductivity of the solid phase k_s can be determined by (Gibson & Charmchi 1997(2))

$$k_s = \frac{k_w \rho_w \varepsilon_{bw} + k_{ds} \rho_s \theta_s}{\rho_w \varepsilon_{bw} + \rho_s \theta_s} \tag{36}$$

where k_w and k_{ds} are the thermal conductivities for water and the dry solid, ρ_s and ρ_w are the densities for water and the dry solid, and θ_s is the dry solid volume fraction. Likewise, the thermal conductivity of the gaseous phase k_g is given by (Gibson & Charmchi 1997(2))

$$k_g = \frac{k_v \rho_v + k_a \rho_a}{\rho_v + \rho_a} \tag{37}$$

where k_v and k_a are the water vapor and dry air thermal conductivities, respectively. Using the volume fractions, the effective thermal conductivity of the entire PM can be stated as (Progelhof et al. 1976)

$$k_{eff} = k_g \varepsilon_g + k_s(\theta_s + \varepsilon_{bw}) \tag{38}$$

Consequently, k_{eff} changes with humidity and the vapor absorption. The form given in equation (38) is known as the series form of the effective conductivity. Some authors use theoretical and semi-empirical formulas, different from the one given above, to model k_{eff}. They suggest that the effective thermal conductivity for highly porous materials will be smaller than that predicted by equation (38), and therefore, an

alternative formula is given. Gibson & Charmchi 1997(1,2) give the following effective conductivity from Progelhof et al. 1976

$$k_{eff} = k_g \frac{(1+\varepsilon_{bw}+\theta_s)k_s + \varepsilon_g k_g}{\varepsilon_g k_s + (1+\varepsilon_{bw}+\theta_s)k_g} \tag{39}$$

This equation is nonlinear in porosity as opposed to equation (38) and results in a lower thermal conductivity for all values of porosity. A plot of typical values (for textiles) of k_{eff} is given in Figure 4. It was found that equation (39) results in about five percent difference in steady state heat flux. Therefore, this difference will be considered acceptable and equation (39) will not be used as the effective thermal conductivity.

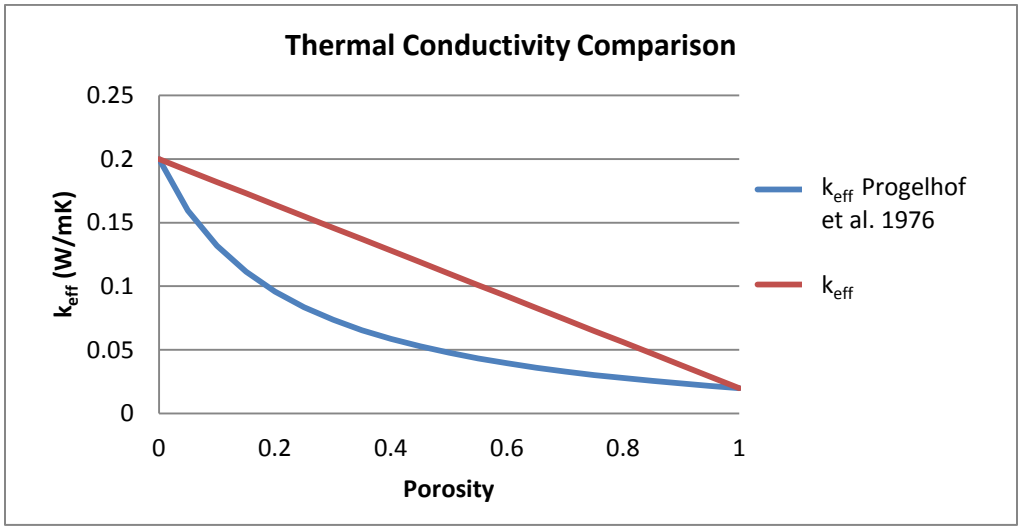

Figure 4. Thermal conductivity comparison

The total density and specific heat of the PM are given by

$$\rho = \varepsilon_{bw}\rho_w + \theta_s\rho_s + \varepsilon_g(\rho_v + \rho_a) \tag{40}$$

$$c_p = \frac{\varepsilon_{bw}\rho_w c_{p,w} + \theta_s \rho_s c_{p,s} + \varepsilon_g\left(\rho_v c_{p,v} + \rho_a c_{p,a}\right)}{\rho} \tag{41}$$

Following the same energy balance as stated in the external flow section, the resulting energy equation for the PM can be written as

$$\rho c_p \frac{\partial T}{\partial t} + \left[c_{p,a}\left(\rho_a \boldsymbol{u}_g - D_{eff}\rho_g \boldsymbol{\nabla}\frac{\rho_a}{\rho_g}\right) + c_{p,v}\left(\rho_v \boldsymbol{u}_g - D_{eff}\rho_g \boldsymbol{\nabla}\frac{\rho_v}{\rho_g}\right)\right] \cdot \boldsymbol{\nabla} T = \boldsymbol{\nabla} \cdot \left(k_{eff}\boldsymbol{\nabla} T\right) + (Q + L)\dot{m} \tag{42}$$

where Q is the heat of adsorption given by Gibson & Charmchi 1997(1,2) and L is the heat of vaporization given as

$$Q = 1.95\ x\ 10^5(1-\phi)\left(\frac{1}{0.2+\phi} + \frac{1}{1.05-\phi}\right) \tag{43}$$

$$L = -2392.2T + 3155500 \tag{44}$$

Figure 5 below is a plot of the heat of adsorption. One can see that this is similar to the sorption relation of equation (24) with the exception that Q decreases with increasing humidity. In this work, a first order polynomial curve fit was performed for discrete heat of vaporization data presented in Incropera, Dewitt, Bergman, & Lavine, 2007. The plot points and polynomial are shown in Figure 6.

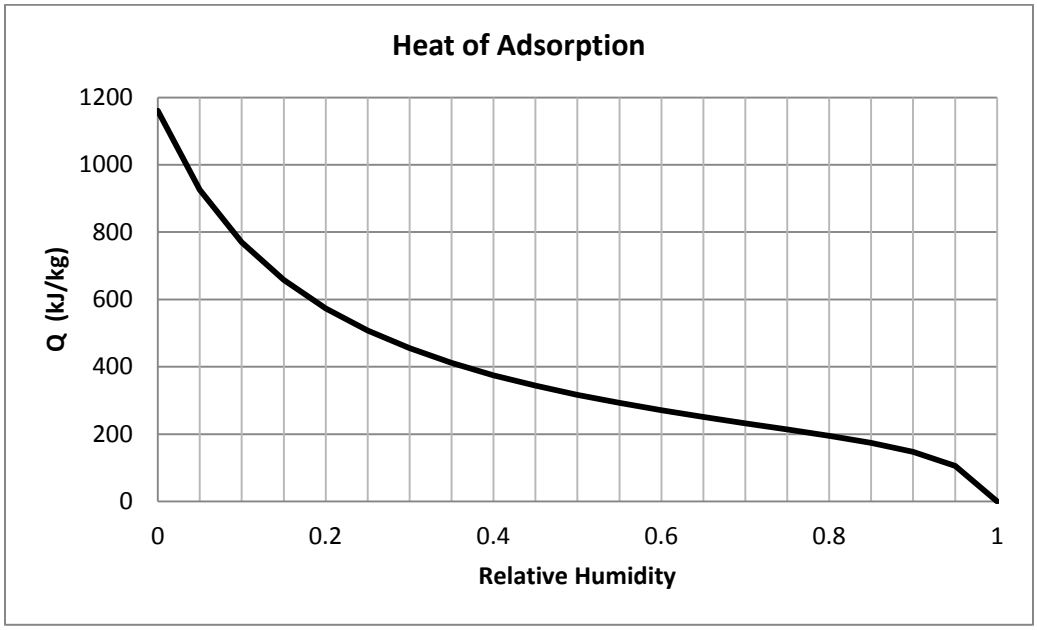

Figure 5. Heat of Adsorption

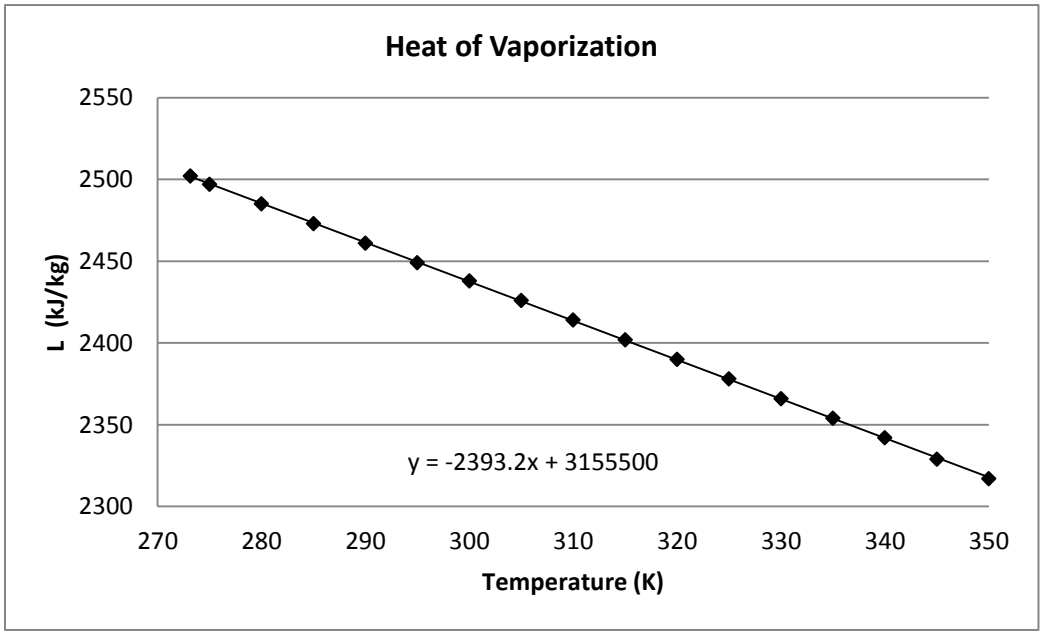

Figure 6. Heat of Vaporization

Chapter 4

Implementation into COMSOL Multiphysics Software

Why Equation-Based Modeling

At the onset of this work, COMSOL's "desktop" interfaces (the physics built into COMSOL) were to be used. During the initial stages of creating the model it was thought that certain physics, such as convective heat transfer inside the PM, could not be modeled with the desktop mode. Therefore, the equation-based approach was started. Even though most of the physics used here can be modeled with the desktop interface, the volume fraction associated with water vapor absorption into the PM would have to be modeled by a user defined equation.

Coefficient Form PDE

Within the PDE interface of COMSOL, there are three different ways to input a PDE. They are: (1) the coefficient form; (2) the general form; and (3) the weak form. The coefficient form was used in this thesis and is the focus of the following discussion. The coefficient form is arguably the most intuitive and easiest form to use since each term in the equation has a coefficient that the user can vary. The form of the equation for a dependent variable u is given as

$$e_a \frac{\partial^2 u}{\partial t^2} + d_a \frac{\partial u}{\partial t} + \boldsymbol{\nabla} \cdot (-c\boldsymbol{\nabla} u - \alpha u + \gamma) + \beta \cdot \boldsymbol{\nabla} u + a u = f \qquad (45)$$

If the dependent variable is defined as a vector with i components then the coefficients will change to accommodate for i components.

Example Using Momentum Equation

We will use equation (31) to show how the equation set of mass, momentum and energy for the external flow and PM (equations (15), (16), (17), (18), (30), (31) and (42)) are implemented in the coefficient form. Repeated here for convenience is equation (31) given as

$$\frac{\rho_g}{\varepsilon_g}\left(\frac{\partial \boldsymbol{u}_g}{\partial t}+(\boldsymbol{u}_g\cdot\boldsymbol{\nabla})\frac{\boldsymbol{u}_g}{\varepsilon_g}\right)$$

$$=-\boldsymbol{\nabla}p+\boldsymbol{\nabla}\cdot\left\{\frac{1}{\varepsilon_g}\left[\mu\left(\boldsymbol{\nabla}\boldsymbol{u}_g+(\boldsymbol{\nabla}\boldsymbol{u}_g)^T\right)-\frac{2}{3}\mu(\boldsymbol{\nabla}\cdot\boldsymbol{u}_g)\boldsymbol{I}\right]\right\}-\frac{\mu}{\kappa}\boldsymbol{u}_g \qquad (31)$$

$$\frac{\partial \rho_g}{\partial t}+\boldsymbol{\nabla}\cdot(\rho_g\boldsymbol{u}_g)=0$$

The second order time derivative term is set to zero for the physics used herein and thus e_a is set to zero. Moving from left to right in the coefficient form, the coefficient of $\frac{\partial \boldsymbol{u}_g}{\partial t}$ is $\frac{\rho_g}{\varepsilon_g}$, therefore, $d_a=\frac{\rho_g}{\varepsilon_g}$. The diffusion coefficient c is $\frac{\mu}{\varepsilon_g}$ and α is zero. In general, the coefficient γ can have x and y components in both the x and y momentum equations. Note that the second viscosity term is multiplied by the identity matrix and so is the pressure. Therefore, can we let $\left(p+\frac{2}{3}\mu(\boldsymbol{\nabla}\cdot\boldsymbol{u}_g)\right)\boldsymbol{I}=\gamma$. Thus, we obtain the respective pressure gradients in each of the momentum equations. The convection coefficient is defined as $\beta=\frac{\rho_g}{\varepsilon_g^2}\boldsymbol{u}_g$. Since no sources or sinks are considered, a and f are also set to zero. In COMSOL the derivatives and partial derivatives of dependent variables are automatically calculated. Therefore, terms such as $\boldsymbol{\nabla}\cdot\boldsymbol{u}_g$ are simple to insert. COMSOL's

notation for a partial derivative of dependent variable u with respect to k, is $\frac{\partial u}{\partial k} \equiv uk$. Hence $\boldsymbol{\nabla} \cdot \boldsymbol{u}_g = ux + vy$. This notation makes the equation-based approach fairly intuitive and enables the user to couple any set of equations.

Solving for Pressure

In this thesis only incompressible flow is modeled, which can present the problem of pressure coupling. When looking at the equation set of momentum and continuity there are two unknowns (velocity components for two dimensions) and thre equations. Generally the pressure for incompressible flow is determined through a pressure correction method or projection method. In order to solve for pressure in COMSOL, one must appeal to the weak form of the equations in which COMSOL uses. The Galerkin weak form uses test functions as basis functions to solve the equations. There is a basis function for each dependent variable and is shown as *test(u)* or *test(p)* for velocity or pressure, respectively. Suppose we integrate equation (45) over the domain, given as

$$\int_{\Omega} \left(e_a \frac{\partial^2 u}{\partial t^2} + d_a \frac{\partial u}{\partial t} \right) dA = \int_{\Omega} \left(\boldsymbol{\nabla} \cdot (-c\boldsymbol{\nabla} u - \alpha u + \gamma) + (f - \beta \cdot \boldsymbol{\nabla} u - au) \right) dA + \int_{\partial\Omega} (BC) ds \tag{46}$$

Therefore, the weak form would be multiplied by the test function, φ=*test(u)*, throughout, to give

$$\int_{\Omega} \varphi \left(e_a \frac{\partial^2 u}{\partial t^2} + d_a \frac{\partial u}{\partial t} \right) dA = \int_{\Omega} \left(\nabla\varphi \cdot (-c\nabla u - \alpha u + \gamma) + \varphi(f - \beta \cdot \nabla u - au) \right) dA + \int_{\partial\Omega} \varphi(BC) ds \tag{47}$$

The requirement is that the above equation must hold for all test functions φ. If the continuity equation is modified to include the dependent variable p (pressure) and is modeled as a source term for pressure, that is

$$0 = -\rho_g \left(\frac{\partial u}{\partial x} + \frac{\partial v}{\partial y} \right) \tag{48}$$

then the weak form would be

$$0 = \int_{\Omega} -\rho_g \left(\frac{\partial u}{\partial x} + \frac{\partial v}{\partial y} \right) test(p)\, dA \tag{49}$$

With this formulation of the continuity equation, pressure can be solved for regardless of time dependency. In fact, this is the same formulation that COMSOL's incompressible flow physics uses to solve for pressure.

Property Equations

All equations that determine properties and relations, such as saturation vapor pressure, solid phase thermal conductivity, and humidity, to name a few, are functions defined outside of the PDE interface. Each equation is defined as an analytical function of a particular dependent variable(s). Therefore, the user can input functions of multiple

variables. An example of this case is the relative humidity. In this thesis ρ_v is taken as the dependent variable for water vapor. Using equations (2) and (8), relative humidity can be written as a function of ρ_v and T and is given as

$$\phi(\rho_v, T) = \frac{\rho_v R_v T}{p_{v,sat}(T)} \tag{50}$$

where $p_{v,sat}$ is a function of temperature, and is another user defined analytical function. The "plot parameters" have to be defined for each variable, which is the range of values the user wishes to use. For this work the specified temperature range is 273K – 325K since subfreezing and high temperatures are not considered. On the other hand, a full range of humidity values are considered. Note that it is possible for the vapor density ρ_v to become negative (due to vapor absorption but at very small values) due to the numerical scheme. In order for all the functions to be defined at all times, the range for ρ_v is allowed to be negative. Therefore the ρ_v range is for -0.01 – 0.1 (kg/m^3), where a value of 0.1 (kg/m^3) corresponds to the saturation vapor density at 325K. To use the function in the PDE interface, we simply call the function by its name with the variables it is a function of, e.g. $\phi(\rho_v, T)$.

Chapter 5

Test Cases

Mesh Refinement

In general in any CFD solution the accuracy of the solution depends on the density of the mesh, which is related to the computational cost. An accurate solution may be obtained but the cost may be very high. In addition, for a finite element scheme, the element discretization can alter the accuracy of the solution. The user can pick the order of element discretization for each dependent variable. However, as the order is increased the degrees of freedom increase accordingly. With high degrees of freedom, the solution will take much longer to solve, especially for time dependent problems. Therefore, one could have a lower mesh count but could increase the order of element discretization for a relatively accurate solution.

Another aspect to consider is whether one should use a structured or an unstructured mesh. Structured meshes tend to conserve mass and energy better than unstructured meshes which makes them advantageous, but the degrees of freedom tend to be higher for the structured mesh solution for the same number of elements. In this work, since certain cases have a rectangular geometry a structured mesh is easy to implement. Thus, a mesh refinement study was performed to determine which mesh type would be most appropriate to use. Note that for the equation-based approach the physics-controlled meshing option cannot be used since COMSOL does not know which physics are being used. Thus, user-controlled meshing has to be employed (for both

structured and unstructured solutions). Figure 7 shows a sketch (not to scale) of the geometry and boundary conditions used for a test problem. The PM is the small rectangle below the flow channel. This setup was chosen so that there would be multiple mass and energy

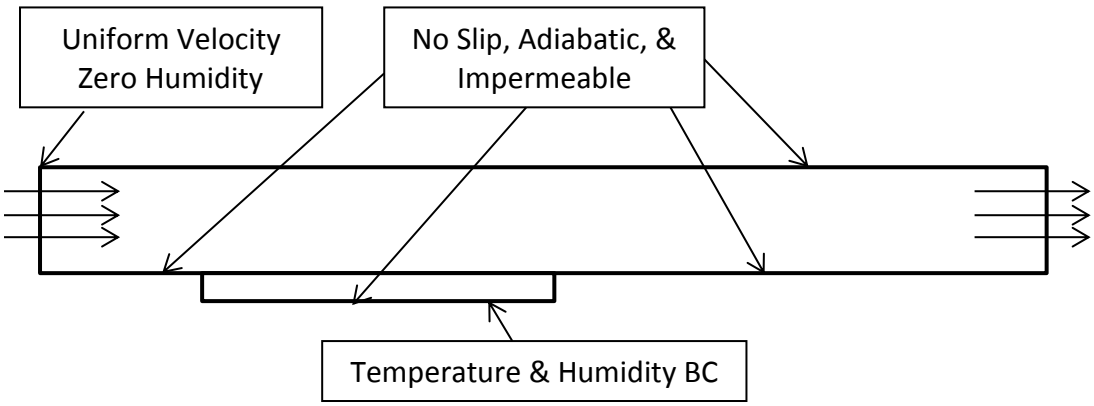

Figure 7. Geometry and boundary conditions for mesh refinement

phenomena involved for a steady state solution. Table 2 shows the results for the study with the type of mesh, number of elements, degrees of freedom (DOF), element discretization together with a measure of conservation of mass and energy. Conservation of mass and energy are measured as the difference of the mass (energy) out of the geometry to the mass (energy) coming into the geometry. For the linear element discretization, all dependent variables are linear except the velocity field, which is kept quadratic (for stability). Similarly for quadratic element discretization, only the pressure is kept linear. Notice that mass and energy are conserved for the structured and unstructured mesh alike for this simple problem.

It was found that for the computational meshes generated, the unstructured types conserve mass and energy with fewer DOF than the mapped types. This can be seen by comparing mesh #2 and #6 from the table. Also mesh #4 and #8 show a similar comparison. Therefore, the unstructured mesh with quadratic elements seems to be the better choice for the types of problems considered and is used in this work. Figures 8 and 9 are the mesh plots for numbers 4 and 9 from the table to give a comparison between the two.

Table 2. Mesh Refinement Results

	Type	Elements	DOF	Disc.	Mass Flux x 10^{-7} (kg/m^2 s)	Percent Difference	Energy Flux (W/m^2)	Percent Difference
1	Mapped	7650	94701	linear	2.912518	0.001567	-2.971718	-0.075738
2	Mapped	9050	111565	linear	2.916296	0.001569	-2.973546	-0.075753
3	Mapped	11600	142681	linear	2.873981	0.001546	-2.978687	-0.075884
4	Mapped	13910	171398	linear	1.922984	0.001034	-2.822407	-0.071905
5	Mapped	17000	209785	linear	1.922984	0.001034	-2.822407	-0.071905
6	UnStrc.	9429	80258	linear	1.829142	0.000984	-2.884812	-0.073475
7	UnStrc.	13581	110960	linear	1.411876	0.000759	-2.722787	-0.069352
8	UnStrc.	20625	165007	linear	1.185528	0.000638	-2.701234	-0.068803
9	UnStrc.	15858	252121	quad.	0.781568	0.000420	-2.632735	-0.067060
10	UnStrc.	20625	296330	quad.	0.775791	0.000417	-2.635064	-0.067119

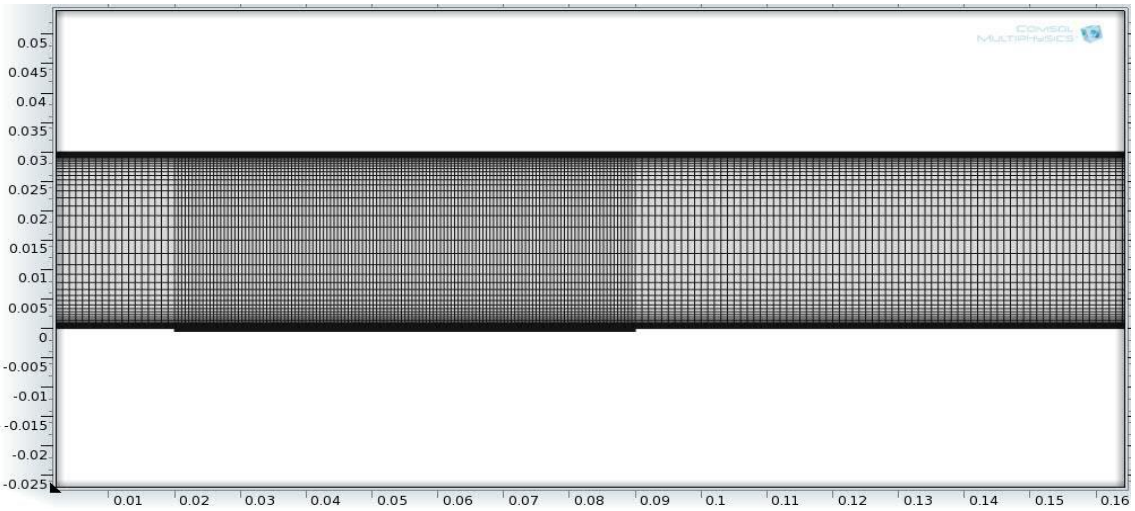

Figure 8. Mapped mesh, #4 from Table 5

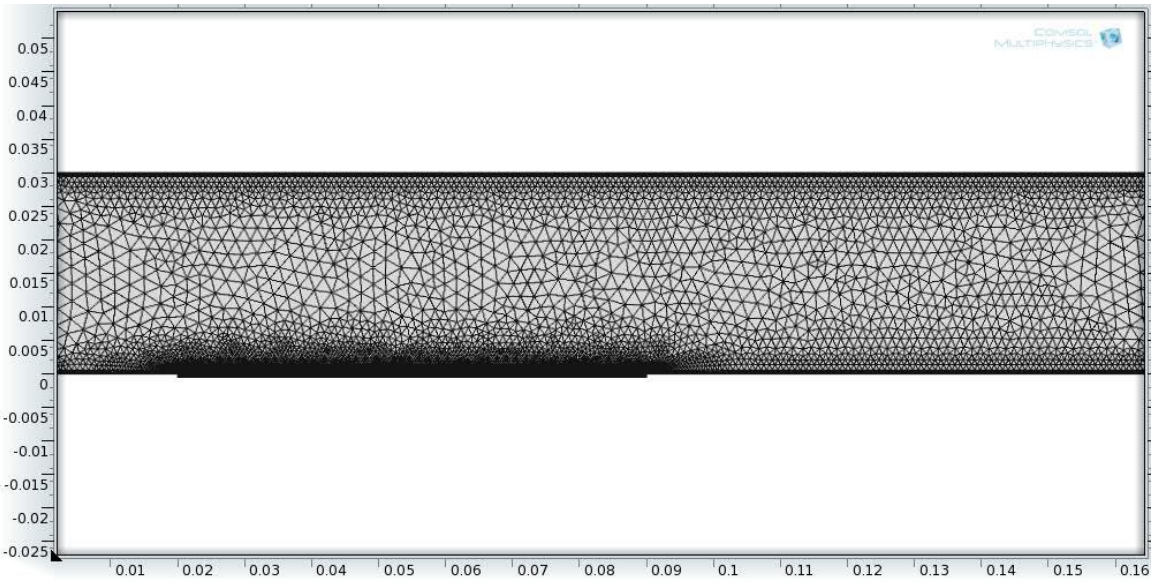

Figure 9. Unstructured mesh, #9 from Table 5

1. Cylinder in Cross-flow

In order to determine if the equation-based approach produces accurate time dependent solutions, flow over a circular cylinder is modeled. Lift and pressure coefficients are computed for the equation-based model and COMSOL's laminar physics module. Both models are solved using the same mesh, element discretization, time-dependent solver, and no numerical stabilization is employed. Below are the initial and boundary conditions used for this problem.

Inlet Condition: Uniform inlet velocity of 0.3 [m/s], $Re_D = 120$

Outlet Condition: no viscous stress, zero pressure

Initial Condition: Zero velocity everywhere

Time Dependent Solver: BDF (backward differentiation formula) with maximum order 2 (for shorter solution time), minimum order of 1. Strict time stepping was used with maximum time step of 0.0025s.

Results

For a cylinder in cross-flow, natural vortex shedding will take place for Reynolds numbers greater than 43 or so. Plots for vorticity magnitude are shown when the flow shedding is initiated (Figure 10) and when the vorticies are well established (Figure 11) for $Re_D = 120$. Typical vortex shedding behavior can be seen from the two figures. These results look reasonable, but the data from lift coefficient will reveal if we are getting accurate results. The lift coefficients in Figure 12 are out of phase very slightly and the PDE formulation has faintly higher amplitude. When the oscillation amplitude becomes

constant, we can see (in Figure 13) that the two solutions are still slighly out of phase but of the same amplitude. This is not a cause for concern since the amplitude and frequency of vortex shedding is what is important once the flow goes periodic.

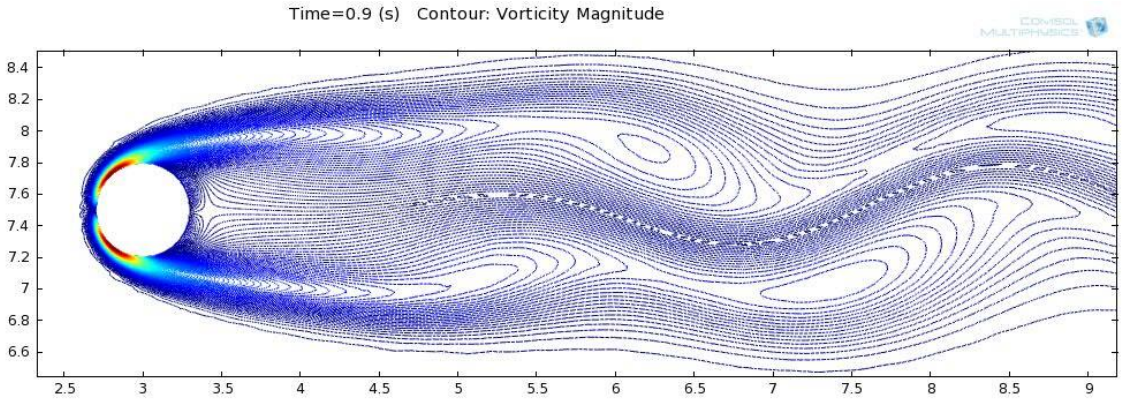

Figure 10. Vorticity magnitude when voticies are forming (axes are in cm)

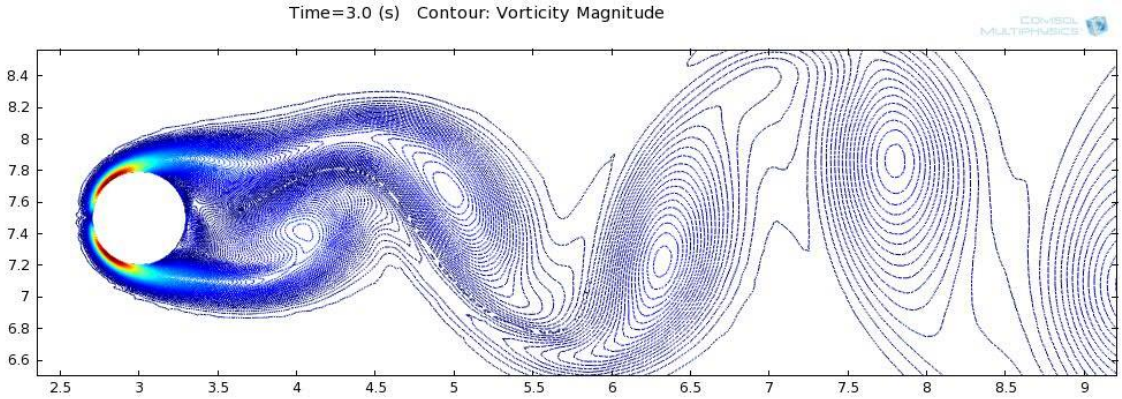

Figure 11. Vorticity magnitude of vortex shedding (axes are in cm)

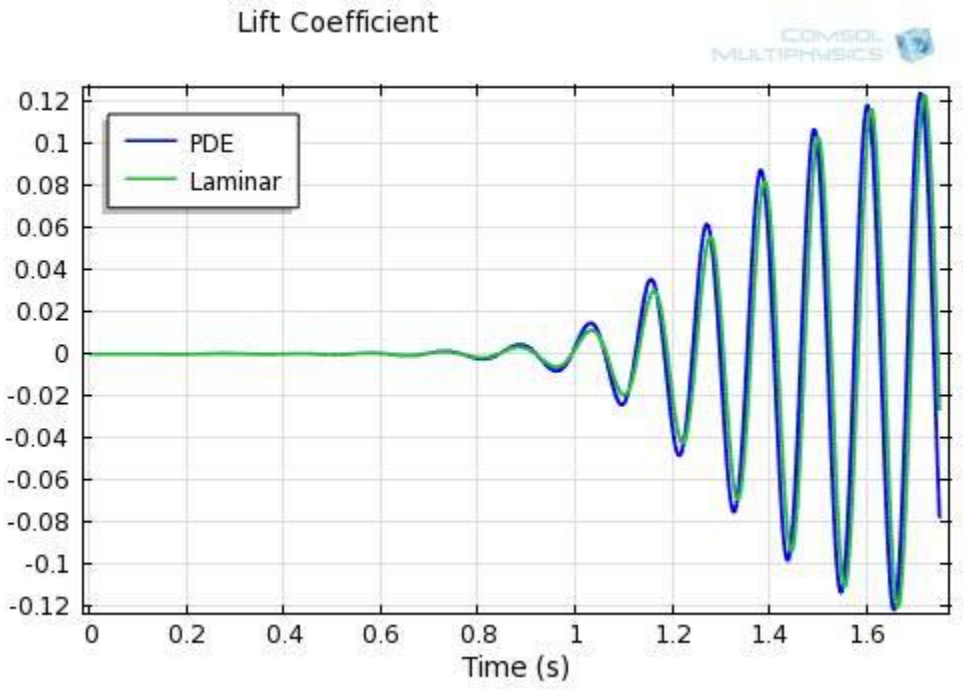

Figure 12. Lift coefficient at start-up

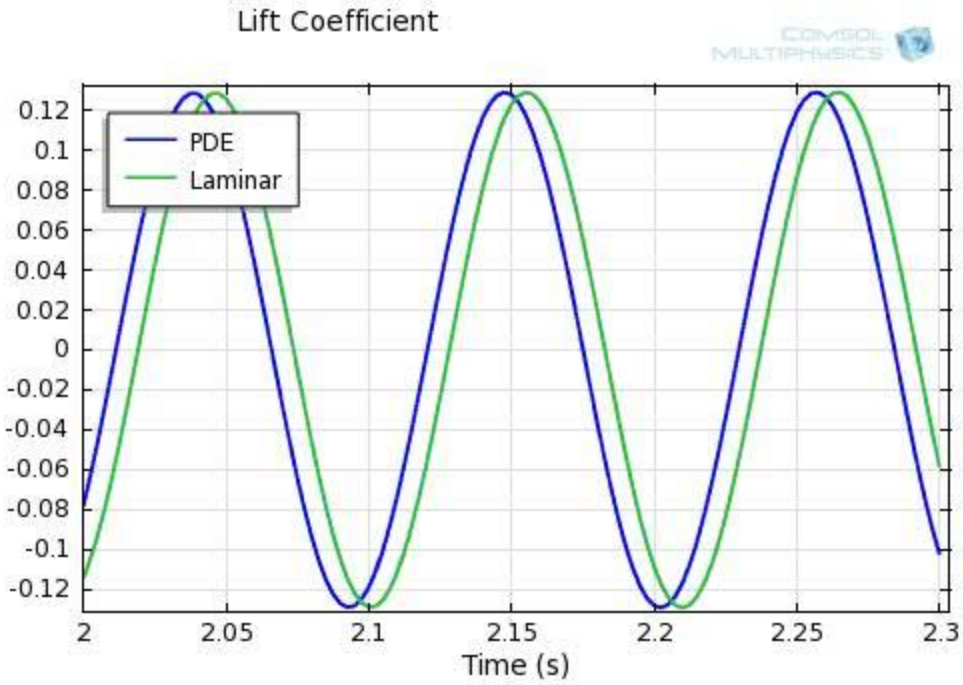

Figure 13. Lift coefficient

Since solving for pressure was of major concern, the pressure coefficient needs to be inspected for similarity. Figure 14 reveals the pressure coefficient on the top half of the cylinder at three seconds. As can be seen, there is nearly an exact match between the two models, namely equation-based and laminar physics.

A last piece of validation that time accuracy is being obtained is to compare the Strouhal numbers for the present work and that of an experimental study. The Strouhal number is a dimensionless number that relates the frequency of vortex shedding with the flow velocity and is given by $St = fD/U$ where f is the vortex shedding frequency, D is the diameter and U is the freestream velocity. Konig & Eckelmann 1998 give a St value of approximately 0.18 for a Reynolds number of 120, which is the case considered here. A Fast Fourier Transform was performed on the data from the numerical simulation and the frequency, shown in Figure 15, was found to be around 9 Hertz. This gives a Strouhal number of approximately 0.18.

From the results presented, the equation-based formulation not only compares with the laminar physics model given by COMSOL, but also produces a solution that compares well with experiments. Therefore, there is confidence in that an accurate flow field can be modeled with this formulation. With that, heat and mass transfer phenomena will be incorporated into the model to investigate additional cases.

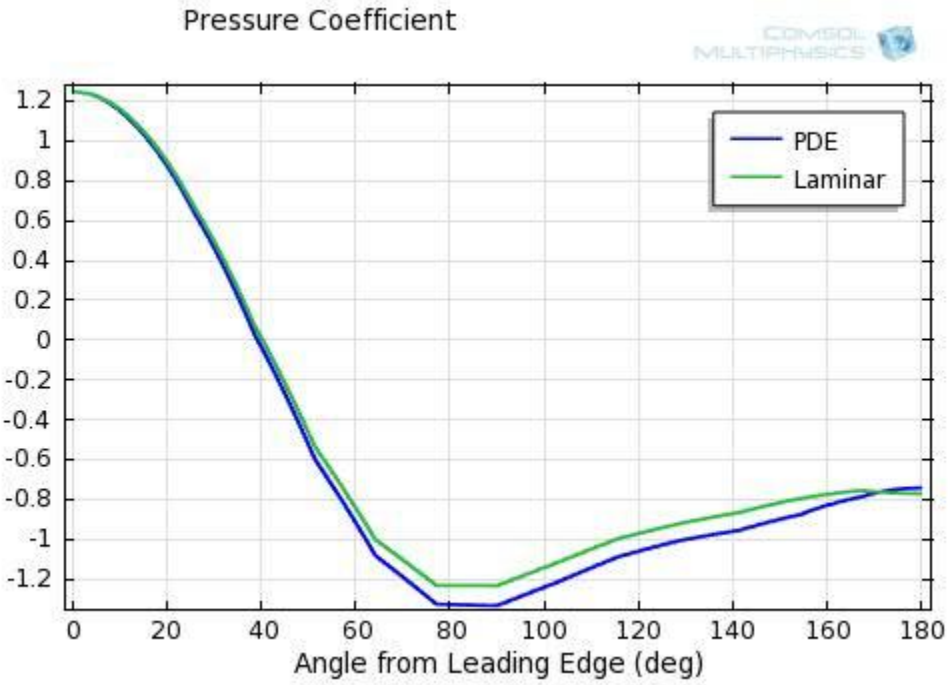

Figure 14. Pressure coefficient at 3 seconds

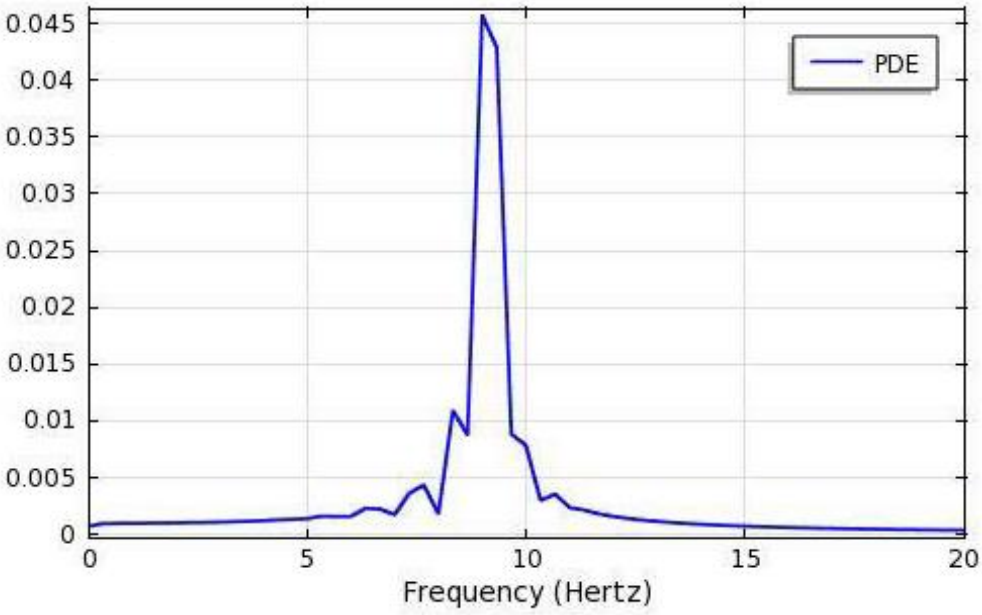

Figure 15. Vortex shedding frequency

2. Diffusion

This simulation models free diffusion and porous medium diffusion in a capillary tube fixed between two bulbs, after the experiments of Davarzani et al. 2010. Although this case is a rather simple one in terms of the physics involved, it is paramount that the formulation for diffusion be validated for porous media. Gaseous mass transfer most often occurs, or is dominated by, diffusion in porous media since most naturally occurring PM are not very porous and thus convection in the medium is considered negligible. Thus the equation to be solved is

$$\frac{\partial C_i}{\partial t} + \boldsymbol{\nabla} \cdot \left(-D_{eff} C \boldsymbol{\nabla} \frac{C_i}{C} \right) = 0 \qquad (51)$$

where we set the tortuosity, τ, be 1.0 since its value is not given.

The computations were performed in three dimensions. The geometry (drawn in 2D) and the boundary conditions are given in the sketch below (Figure 16). In the middle of the tube is the valve in the experimental setup. For the model developed herein, the valve is simply a line that divides the tube in half.

Initial Conditions: Each gas is given a concentration equal to 100 [mol/m^3] which reflects that 100% of that gas occupies its respective bulb. It must be noted that, we assume 100% concentration of the gas up to the valve. That is, there is 100% helium in the top half of the tube and 100% nitrogen in the bottom half of the tube. The binary diffusion coefficient used for He and N_2 is 0.70 [cm^2/s], which is the value determined from the experimental data. When the PM is inserted, it is placed in the bottom 4 [cm]

of the tube, just above the N_2 bulb. Even with the PM inserted the initial conditions of gas concentration were unchanged, which means that the PM is initially saturated with N_2.

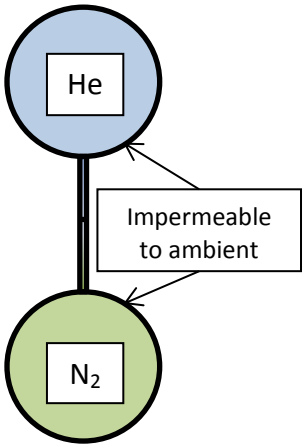

Figure 16. Geometry and boundary conditions for diffusion simulation

Results

Figure 17 presents the results from the present simulations and experiments. As can be seen, the free diffusion data matches very well. Therefore, it can be said that the diffusion equation and numerical scheme give an accurate solution for this problem. We can assume that modeling for a PM would give similar results, but our results for diffusion in the PM are not as well matched. The percentage of N_2 calculated in the bulb is about 1.5 – 2% less than the experiments. From the experiments, an effective diffusion coefficient is calculated for the entire system (not to be confused with the effective diffusion coefficient for a PM alone) based on curve fitting. The same was done in the numerical simulation and Table 3 presents those results. We can see that there is a difference in

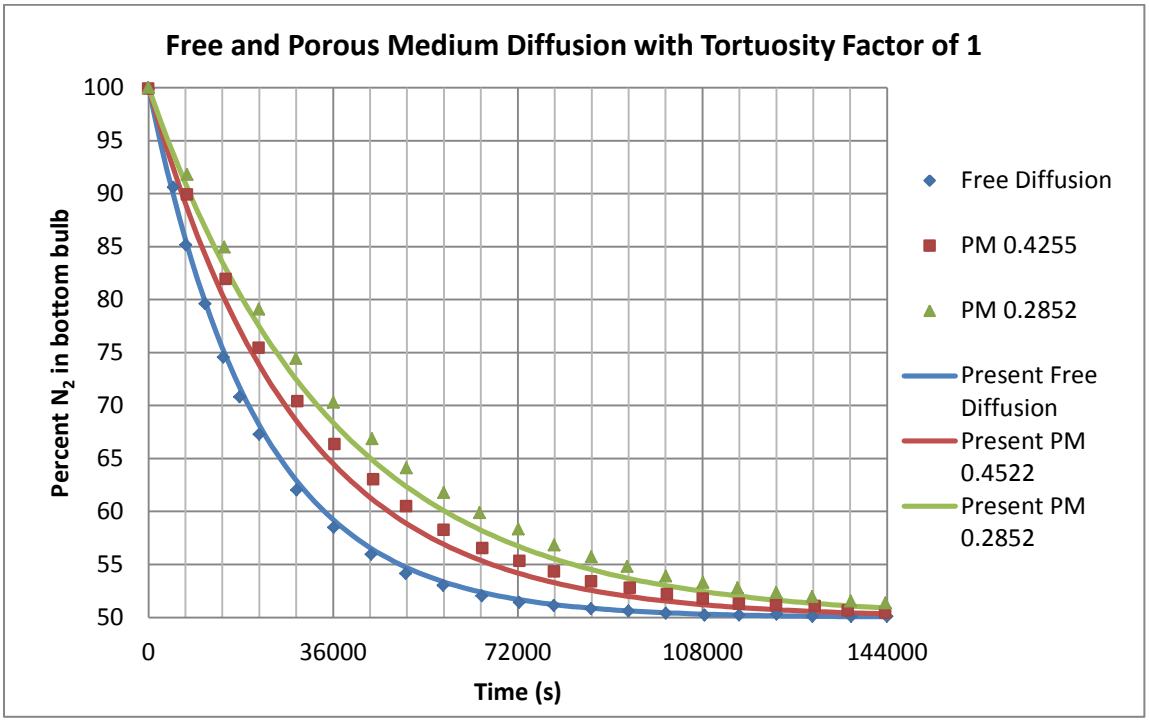

Figure 17. Results for free and porous medium diffusion

the effective diffusion coefficients determined numerically and experimentally. Recall that since a tortuosity factor is unknown for this PM it was kept at a value of one. The results in Table 3 suggest that a different tortuosity factor could be used since the numerical effective diffusion coefficient is higher than that of the experimental. Therefore, a tortuosity factor was sought numerically to verify this theory. If the tortuosity $\tau = 1.2$ is used the results in Figure 18 for both PM match very well.

What this shows is that the effective diffusion coefficient defined in equation (23) may lead to physically correct results. With the diffusion physics and the form of the diffusion coefficient verified, we can now proceed and add more physics. A logical

next step is to include convective flow and investigate the effects of combined diffusion and convection through a PM.

Table 3. Effective Diffusion Coefficients for System

Effective Diffusion Coefficient for System			
Porosity	**Exp.**	**Present**	**% Difference**
0.4522	0.438	0.49	11.87
0.2852	0.355	0.395	11.27

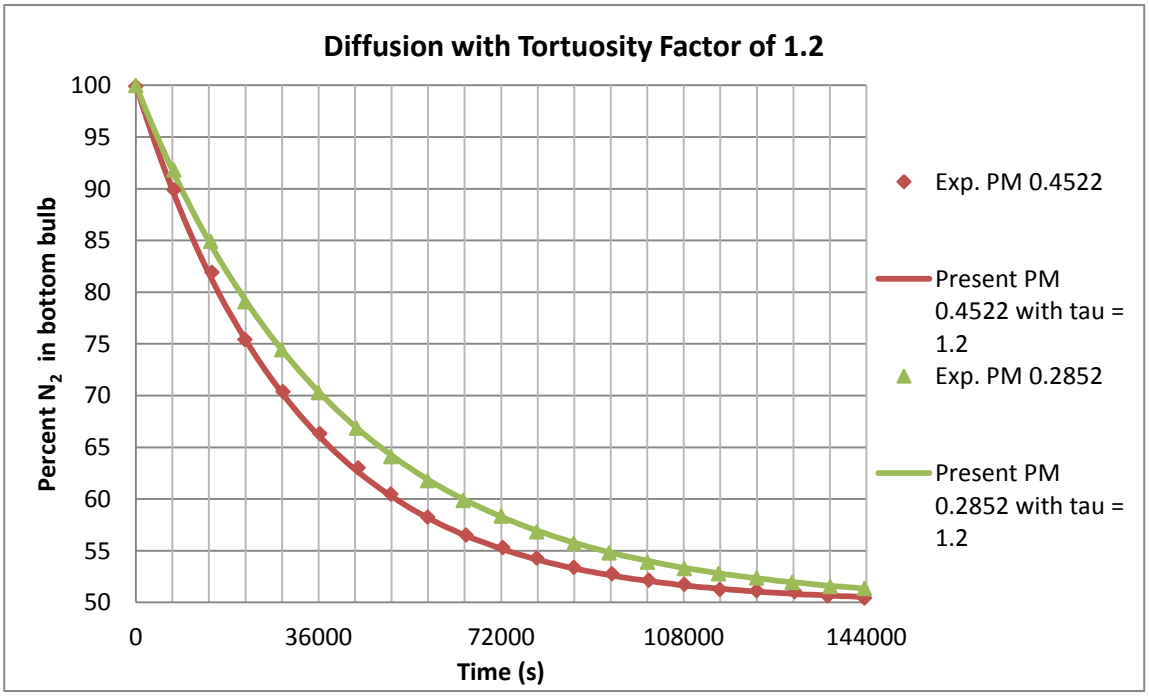

Figure 18. Diffusion with tortuosity factor of 1.2

3. Steady State Convection and Diffusion

To examine moisture diffusion and convection in porous media, a simulation of a PM in a parallel flow channel, modeled after the work of Gibson & Charmchi 1997(2), will be used. A non-hygroscopic material (polyester) and a hygroscopic material (cotton) will be modeled. Polyester and cotton are the fabrics of choice because they are typically apparel and have remarkably different characteristics.

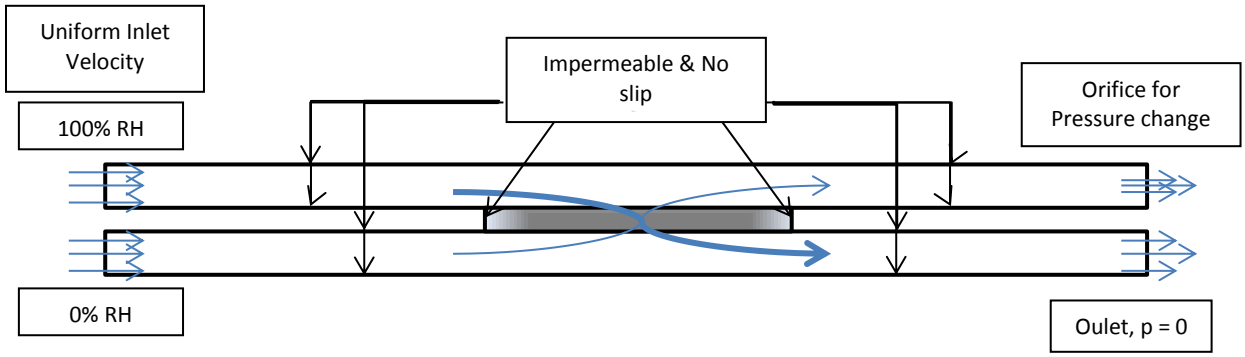

Figure 19. Geometry and boundary conditions for parallel flow simulation

Above is a sketch of the geometry and boundary conditions used (not to scale). It consists of an upper and lower flow channel with the PM sandwiched in between. In the middle of the channels on the bottom and top walls there is a gap for the PM surface to be placed. This arrangement allows the air to pass through the PM. If the pressure across the PM is zero then there is no convective flow through the PM due to symmetry. If a pressure difference is created a net flow (either up or down) through the medium will occur. A pressure difference is used to do precisely that. If we let the pressure

difference $\Delta p = p_{top} - p_{bottom}$ where p_{top} and p_{bottom} are the average pressures along the top and bottom surface of the PM, respectively, then a positive pressure difference is a higher pressure on the top and vice versa. This higher pressure is created by an orifice at the exit of the channel which is regulated by a parameter for the size of the opening. For high pressure on the bottom the same orifice is used at the bottom exit while the top exit is kept fully open. Note that the actual experiments were set up in three dimensions where the channel exits are surfaces. Also, the orifice geometry is unknown and is modeled here as a rectangular opening at the exit surface.

All simulations are performed using the steady state flow physics. By varying the orifice opening, a parametric study can be performed to change the geometry in order the get a pressure difference. In all computations presented herein, an unstructured mesh was used because of this geometry change. The relevant properties of each material are given in Table 4. Permeability for each material is based on the flow resistance mentioned earlier in the PM conservation of momentum section. Since cotton is hygroscopic, its permeability as well as its porosity will vary which should restrict the flow through the PM.

Table 4. Material Properties

	Dry Porosity	Permeability (m^2)	R_{sat}	Thickness (m)
Polyester	0.707	2.61×10^{-11}	0.00	5.89×10^{-4}
Cotton	0.664	variable	0.0622	3.84×10^{-4}

Results

Figure 20 shows the plot for dimensionless velocity magnitude at the inlet with streamlines in white, whereas Figure 21 show the velocity field with streamlines for the porous medium. As expected, the streamlines are strictly horizontal everywhere since no vertical pressure gradient exists. Accordingly, the plot of pressure in Figure 22 is symmetrical about the x-axis.

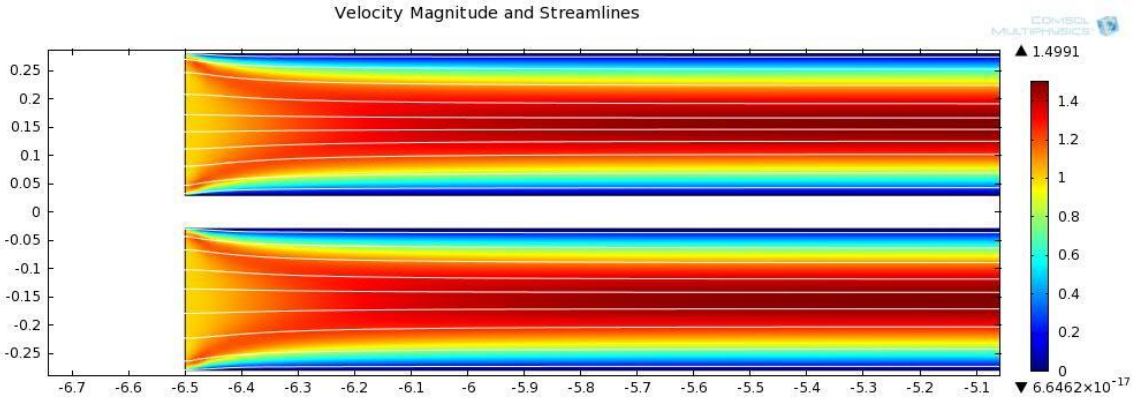

Figure 20. Velocity magnitude and streamlines at the inlet (axes are in cm)

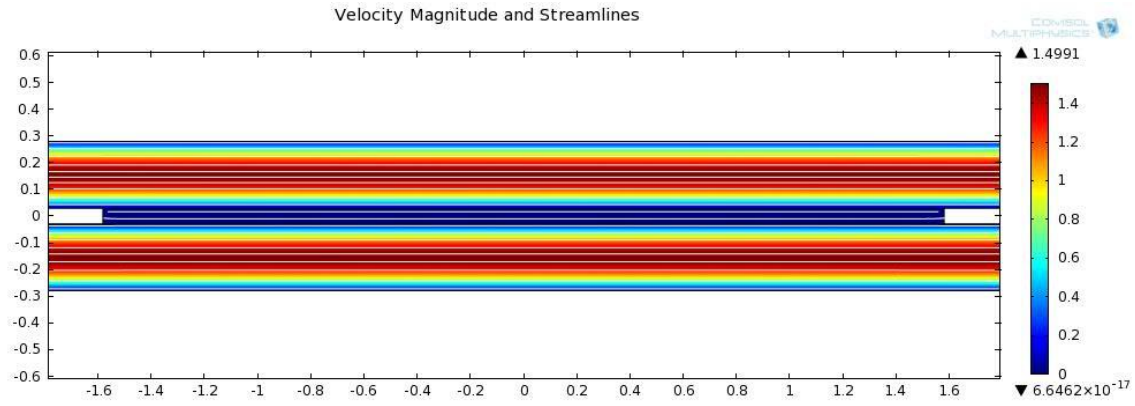

Figure 21. Velocity magnitude and streamlines for channels and PM (axes are in cm)

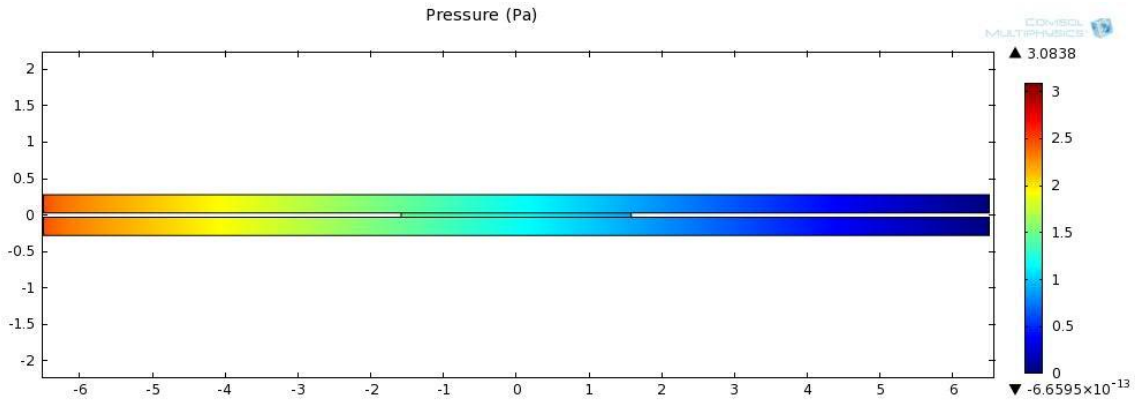

Figure 22. Pressure for fully open channels (axes are in cm)

From the relative humidity plot given in Figure 23, one can see the presence of diffusion in water vapor. Even though there is essentially no convective flow normal to the PM, water vapor still passes through it. The question to ask is, “is this the realistic amount of water vapor that should be diffusing through the PM?”. This question will be addressed later.

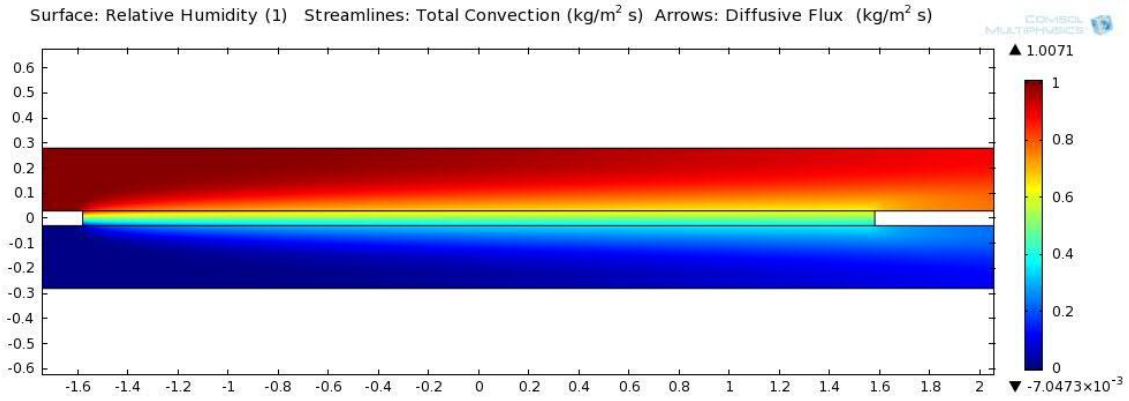

Figure 23. Relative humidity through the PM (axes are in cm)

In Figure 24 below, the total convection is shown as streamlines, which is the combination of diffusion and advection, while the arrows are just the diffusive flux. Since the normal component of the velocity is zero in the PM, convection is dominated by diffusion there.

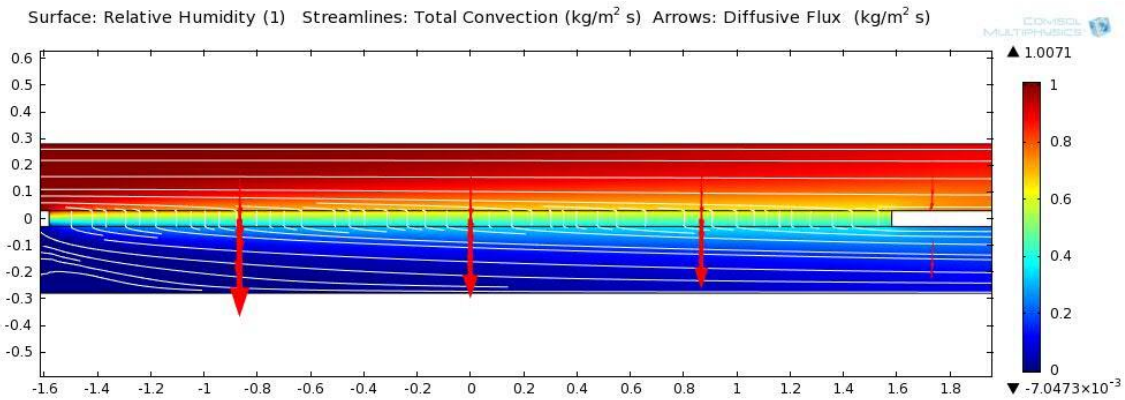

Figure 24. Relative humidity with total convection streamlines (axes are in cm)

At the other extreme, when the orifice is small and higher pressures (Figure 26) exist in the upper channel, water vapor is advected through the PM along with the diffusion as seen in Figure 25. The bottom average humidity is higher as expected. To see the velocity increase in the PM, velocity magnitude at the center of the PM is plotted in Figure 27 with each change in the orifice. The x-axis is the orifice parameter where a small value corresponds to a small orifice.

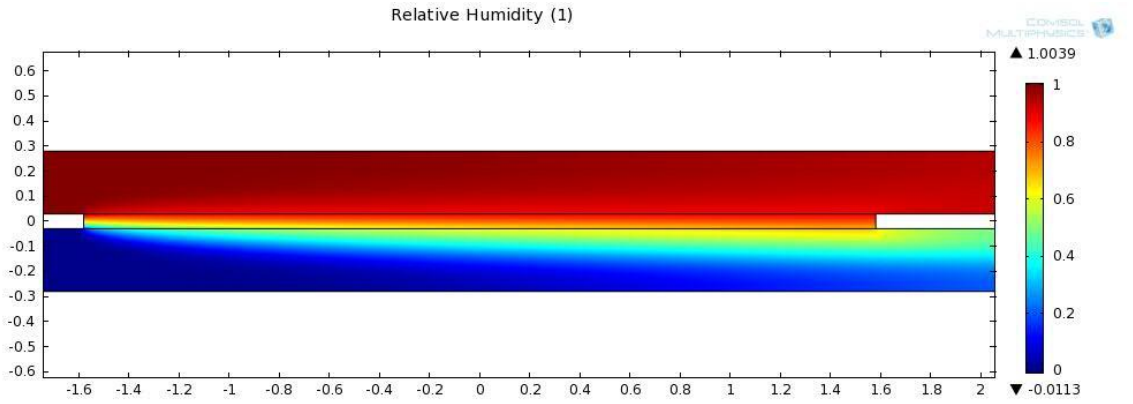

Figure 25. Relative humidity when the orifice is 10% open (axes are in cm)

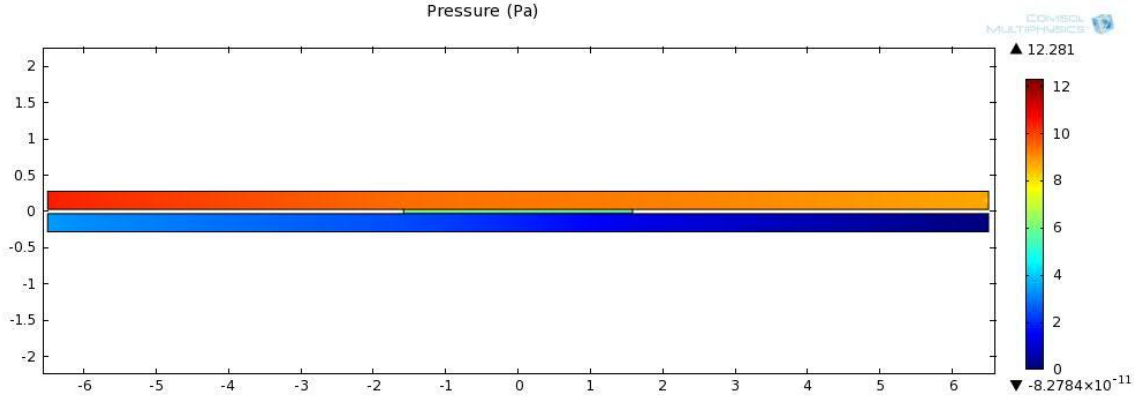

Figure 26. Pressure when orifice is 10% open (axes are in cm)

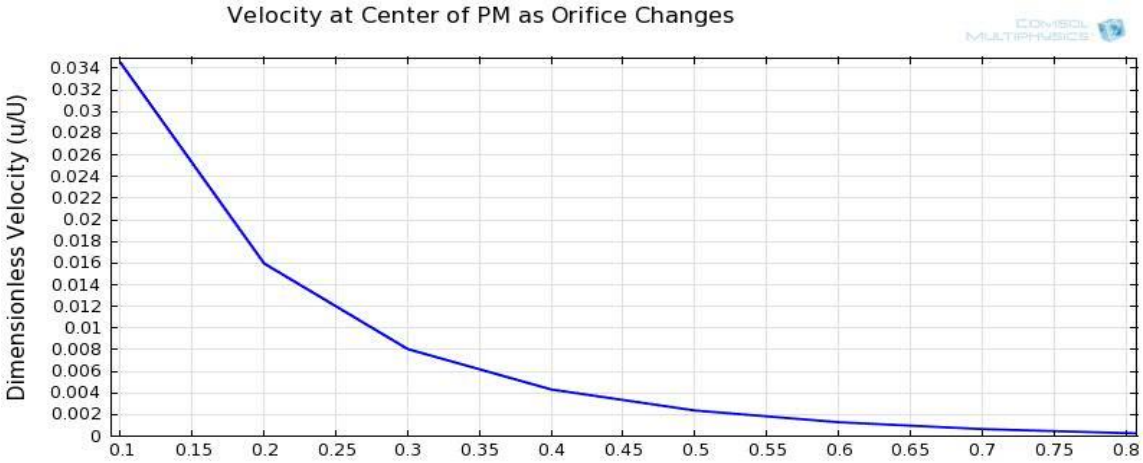

Figure 27. Velocity magnitude at the center of PM

Figure 28 above shows the velocity profiles at mid-length which includes the channels and PM. The profiles are for velocity magnitude which can make the profile in the PM seem as though there is a slight uniform flow in the streamwise direction. This is not the case, in fact the velocity in the PM when the orifice is small (green curve) is almost entirely normal (v component) to the PM.

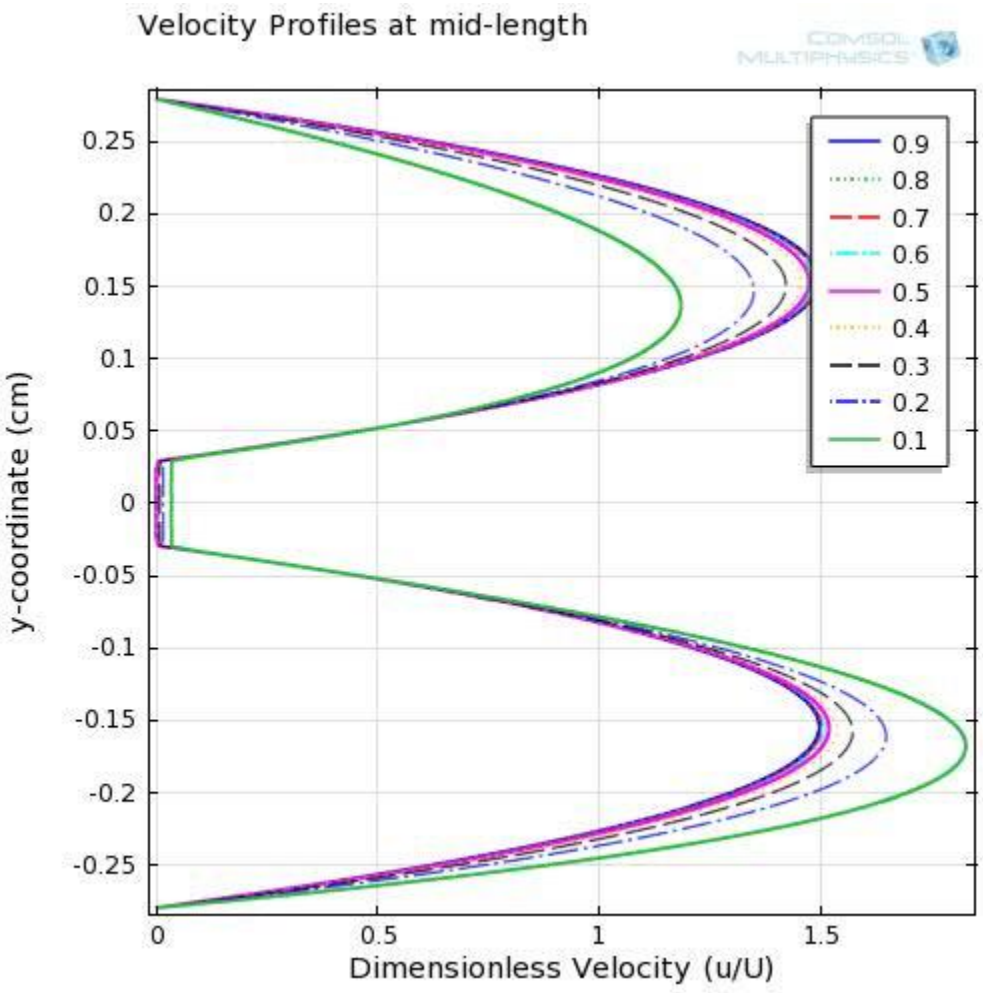

Figure 28. Velocity profiles at mid-length

Regarding the question posed earlier about the water vapor flow through the PM, Figures 29 and 30 compare our results with those of Gibson & Charmchi 1997(2). Shown is the relative humidity at the bottom exit as a function of pressure difference across the PM. Figure 29 is for a non-hygroscopic material, namely polyester and Figure 30 is for cotton, which is hygroscopic. The results for both cases compare well with the numerical work of Gibson & Charmchi 1997(2).

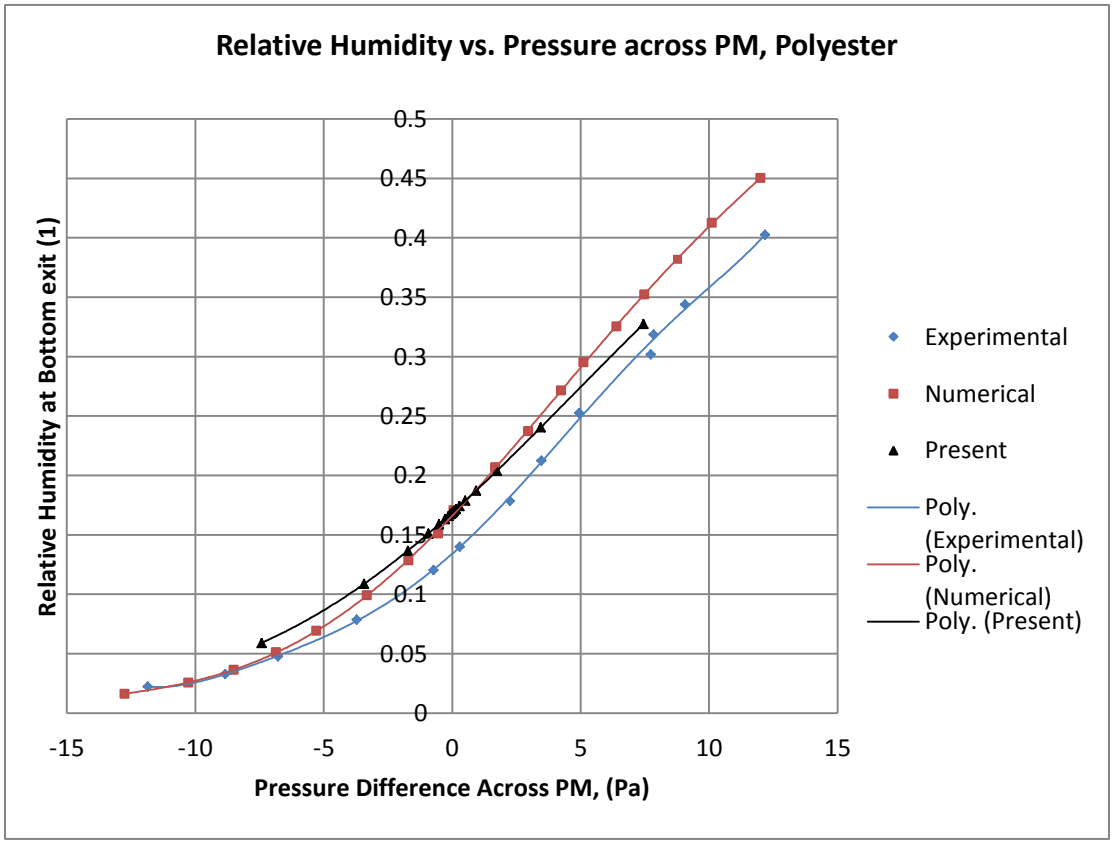

Figure 29. Humidity at bottom exit for pressure differences across PM for polyester

Agreement with the experimental data is not quite as good as the numerical results but the overall characteristics are well-captured. The results are very similar for zero pressure difference with deviations as the pressure increases. Also notice that compared to Gibson & Charmchi's numerical results, the present results under predict the humidity and over predict the humidity for positive and negative pressures, respectively. This may be due to the different governing equations used for the flow fields. Gibson & Charmchi 1997(2) use Darcy's Law for the flow field in the PM while Brinkman's extension of Darcy's Law was used in the present work. It is possible that as the pressure difference increases, the inertia terms in the present formulation may start to dominate.

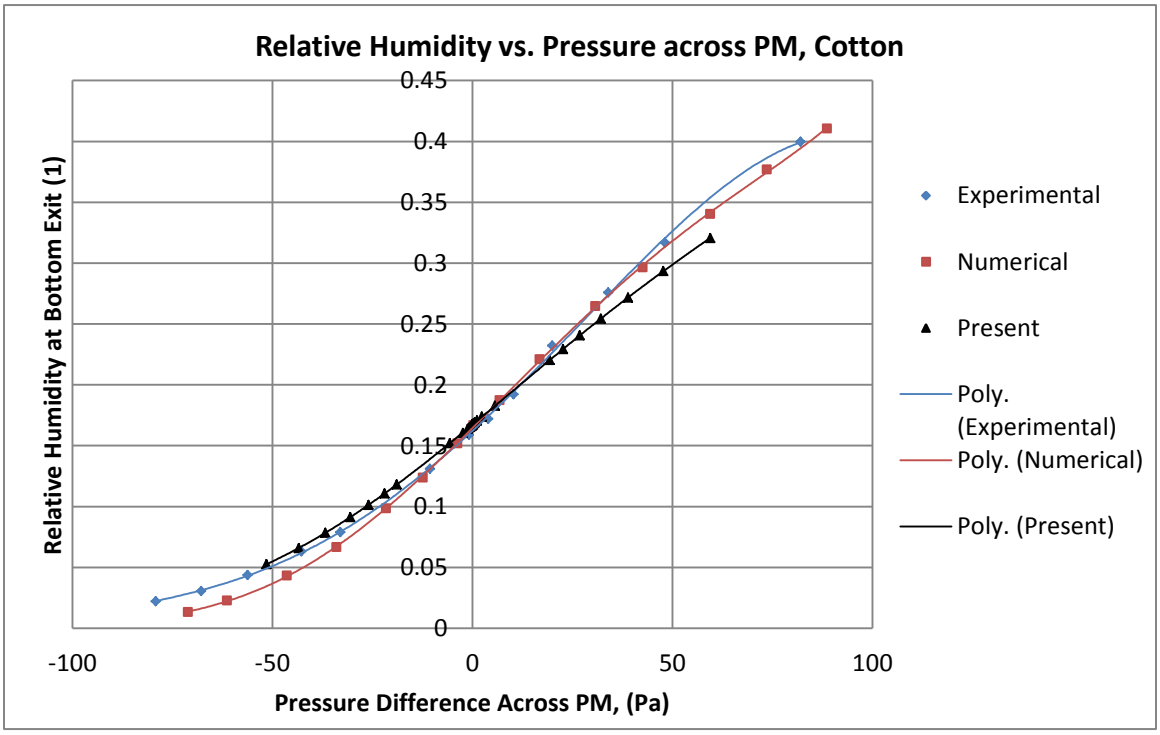

Figure 30. Humidity at bottom exit for pressure differences across PM for cotton

Notice that for cotton it takes a higher pressure difference to achieve the same exit humidity as polyester. This is partly due to the difference in porosity (0.707 and 0.664 for polyester and cotton, respectively), but mainly due to the permeability change for cotton as the fibers swell. It can be deceiving that the cotton data matches as well as the polyester at high pressures. It is important to realize that the pressure scale in each is different. Particularly for polyester, notice the rise in exit humidity as the pressure increases. From the present work, the humidity increases from about 17% to 33% when the pressure increases from 0 to 7.5 Pa. In terms of mass flux from the bottom surface of the PM, this is a 123% increase in water vapor mass flux. Recall that (see Figure 27) the velocity in the PM was approximately 3.4% of the inlet velocity for the smallest orifice size. Although the velocity was small, the mass flux increased by 123%. This means that small normal (normal to PM) velocities have an appreciable effect on the mass flux. A similar mass flux increase is seen for cotton except that higher pressure is needed because of the swelling of the fibers, as state before. What this simulation does not show is how the energy of the PM changes as the water vapor is absorbed into the medium. The following case will explore these transient effects.

4. Vapor Absorption

Since a time accurate solution can be obtained, the following time dependent test case is used to compare the transient aspects of absorbing porous media. Comparison is made with Gibson & Charmchi 1997(2) (same as the above test case) where the temperature in the PM will be the focus. A dry specimen will be suddenly subject to a one hundred percent humidity air flow. As the moist air comes in contact with the material it will be absorbed and energy will be released resulting in a temperature increase. As the mass flow into the fabric decreases and since convective heat transfer is present, the temperature will decrease down to the ambient temperature. Conditions and properties for the simulation are given below.

Initial Temperature: 293K everywhere

Initial Velocity and Humidity: zero everywhere

Temperature inlet: Initial Temperature of 293K

Humidity inlet: 100% for both the top and bottom channels

Velocity inlet: uniform flow

Table 5. Properties for Cotton Fabric

k_{ds} (W/mK)	ρ_s (kg/m^3)	$c_{p,s}$ (J/kgK)	ε	τ	R_{sat}
0.16	1550	1210	0.664	2.12	0.0622
		D_S (m^2)	d_f (m)		
		1.50×10^{-13}	3.60×10^{-6}		

For this case, the equilibrium regain is determined by

$$R_{eq} = 0.011\frac{8\phi}{1+8\phi}\left[\frac{1-0.81\phi^5-(1-0.81)\phi^{16}}{1-\phi}\right] \quad (52)$$

where its parameters are $R_0 = 0.011,\ k = 8,\ a = 0.81,\ n = 5,\ m = 16$ when this relation is matched to equation (24). Note that in the work of Gibson & Charmchi 1997(2) the fiber diffusion coefficient D_s and fiber diameter d_f were not given. However, Gibson & Charmchi 1997(1) provide properties for cotton in a different paper. They gave a value for $D_s = 4.0x10^{-14}(m^2)$ and $d_f = 3.6e^{-6}(m)$. Using the given fiber diameter and the diffusion coefficient given in Table 5 the numerical results compared well with the experimental results.

Results

Figure 31 is a humidity plot at 0.2 seconds just as the moist air front has passed by the PM. Figure 32 is a humidity plot of a non-hygroscopic material at the same time with all the same conditions. It can be clearly seen that the hygroscopic material is absorbing the water vapor since the humidity in the PM is less than that of the non-hygroscopic material everywhere.

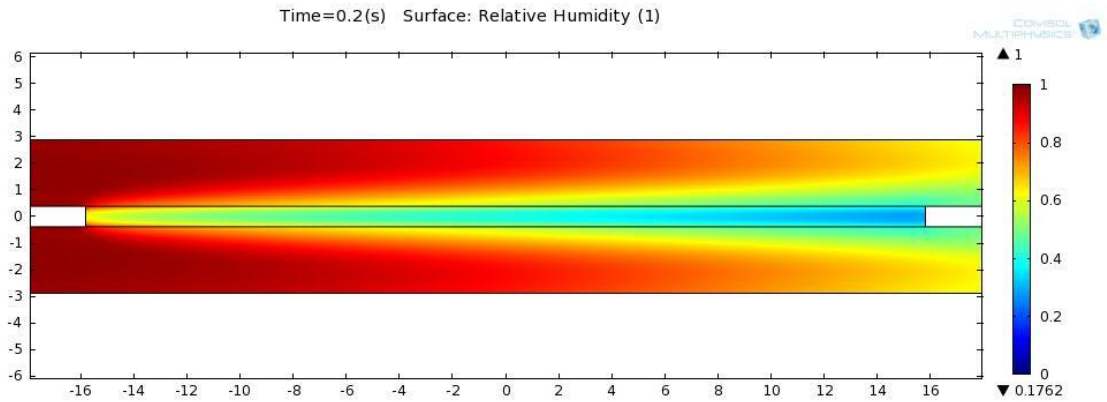

Figure 31. Humidity of hygroscopic material after 0.2 seconds (axes are in cm)

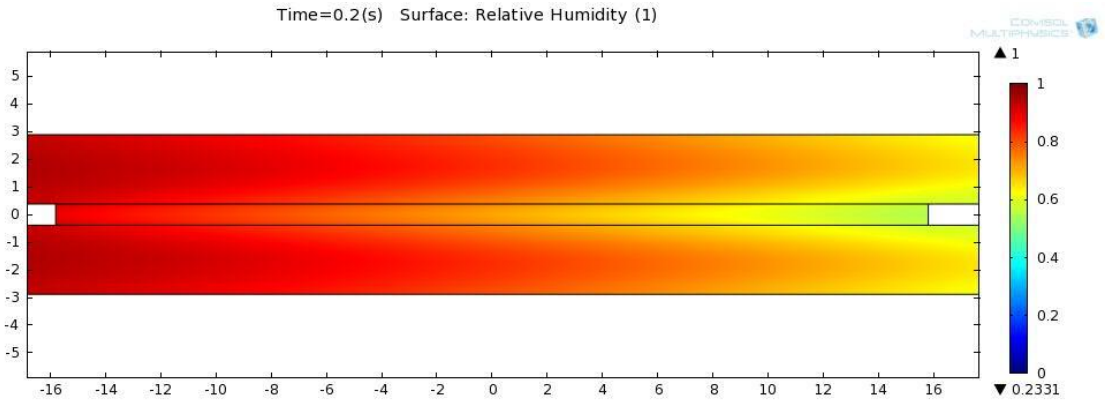

Figure 32. Humidity of non-hygroscopic material after 0.2 seconds (axes are in cm)

With the absorption of water vapor, energy is liberated in the form of heat. Since the leading edge of the PM is subject to the moist flow first, the temperature there will initially rise as seen in Figure 33. Note that the temperature range in Figure 33 is small (293-293.3 K). This scale was used so that temperatures could easily be seen. Since the fibers at the outer edges are subject to higher humidity, which yields a higher mass flow potential into the fibers, the temperature there will be higher. The middle of the medium is not subject to higher humidity yet partly because of the absorption of the outer fibers. As stated earlier, the regain at the outer edges is higher than that in the middle at this early stage. Figure 34 reveals this behavior at the leading edge after one second. In addition, Figure 35 shows the temperature field at one second. By this point, the temperature is nearly uniform in the vertical direction. Since there is convective heat transfer, the leading edge temperature begins to drop, which is a consequence of the conjugate modeling as the heat transfer coefficient is highest at the leading edge.

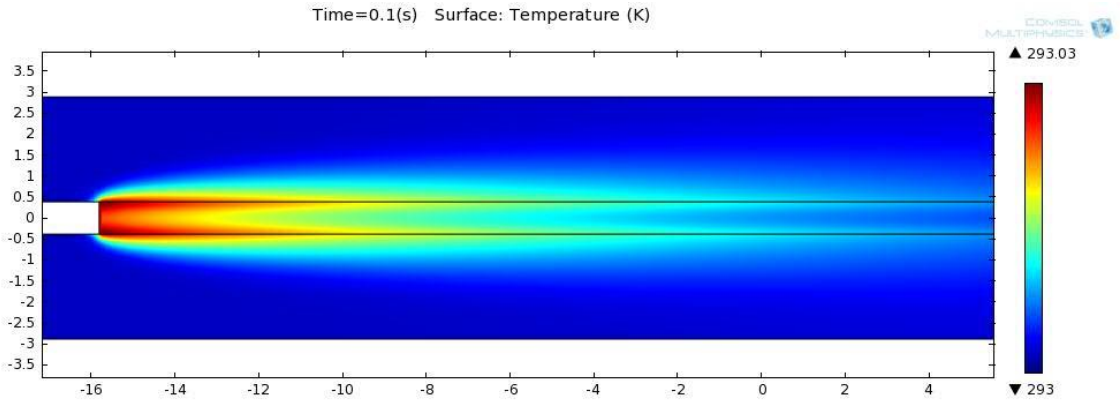

Figure 33. Temperature field in PM after 0.1 seconds (axes are in cm)

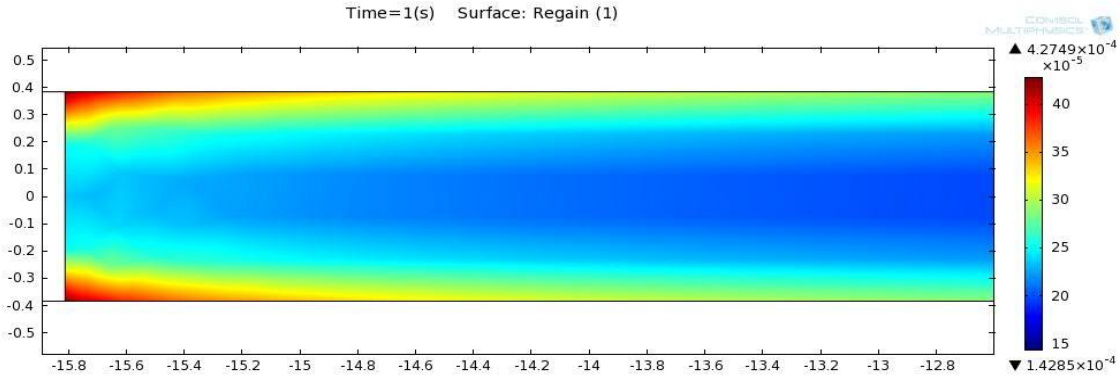

Figure 34. Regain in PM after 1 second (axes are in cm)

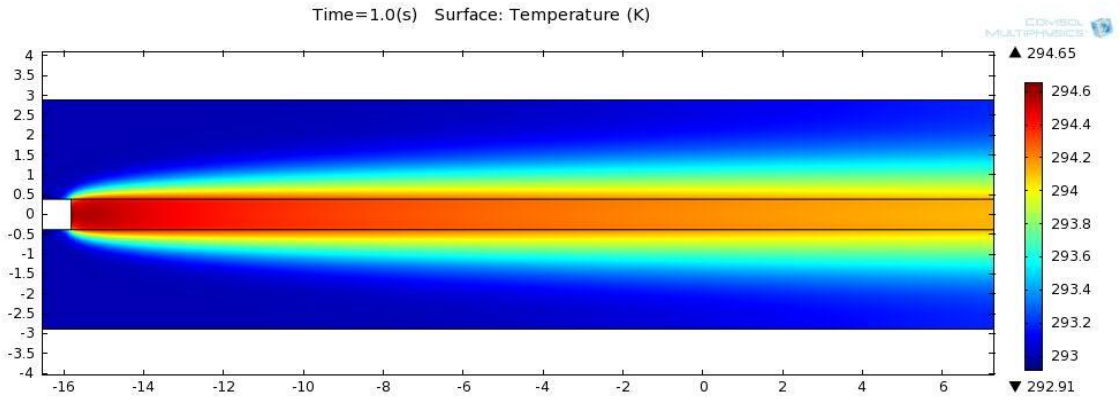

Figure 35. Temperature field after 1 second (axes are in cm)

Figures 36 – 39 give results for quantities that change over time in the PM. First is the humidity and we can see that at approximately 25 seconds there is a sudden decrease. This is because the temperature suddenly rises at the same instant. If the vapor concentration is constant and the temperature rises, then relative humidity decreases. The vapor absorption is the other contributing factor to the decrease in humidity, but mostly the absorption keeps the humidity from increasing quickly.

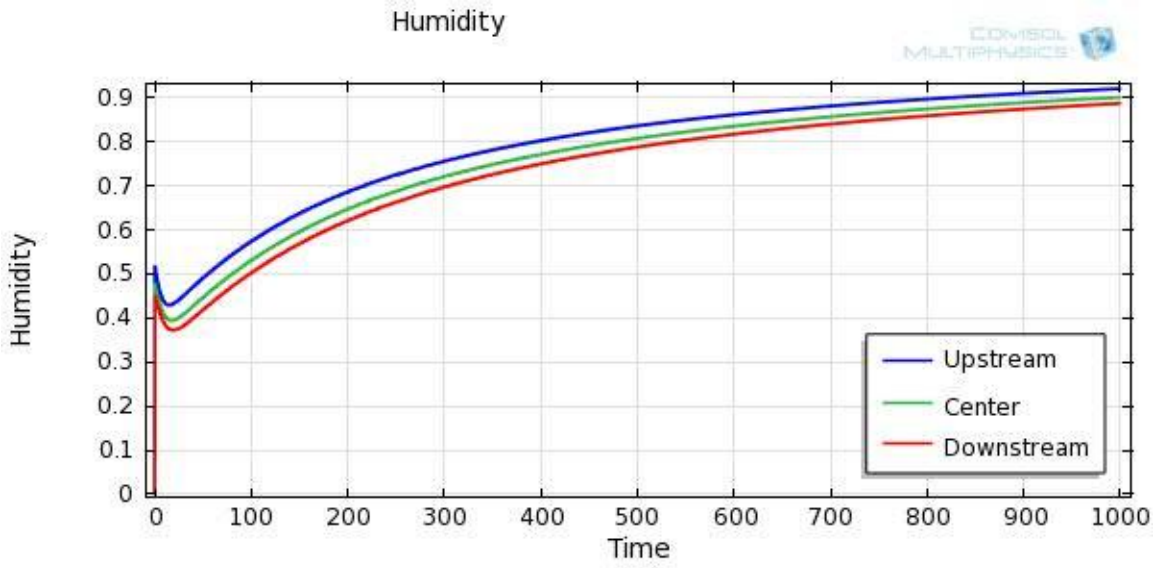

Figure 36. Humidity over time in PM

The regain plot shown in Figure 37 smoothly increases as time progresses, but the rate of increase drops. This is expected since the potential for mass flow is the difference of the equilibrium regain and the regain of the fiber. As the fiber absorbs moisture, that potential decreases. Consequently, the mass flow also decreases. As a

matter of fact, the mass flow will be at a maximum initially and then decay to zero at steady state. Figure 38 shows this change in mass flow.

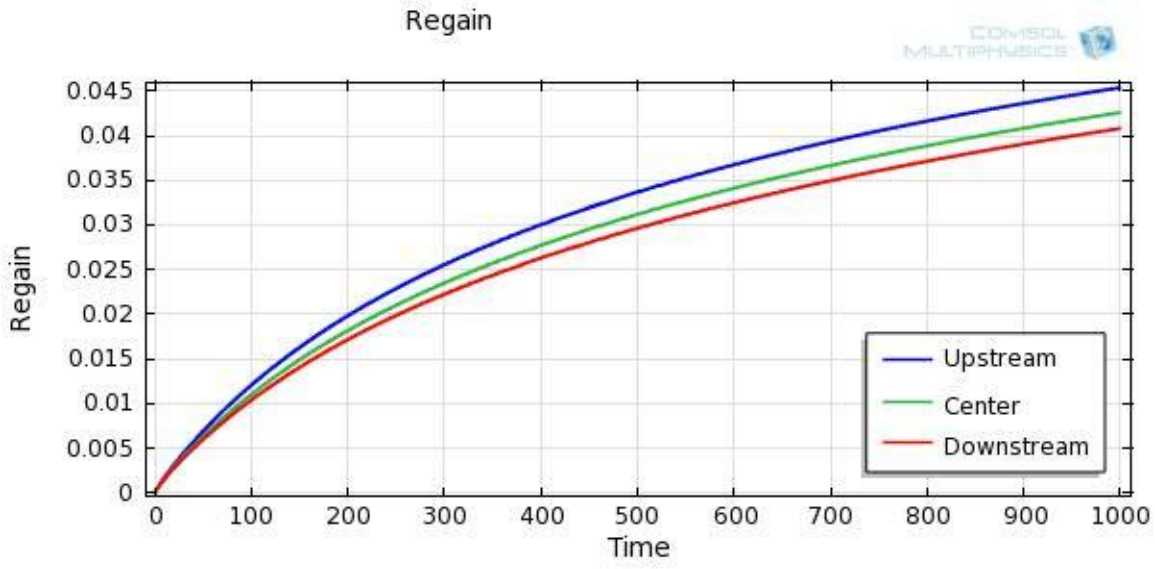

Figure 37. Regain over time in PM

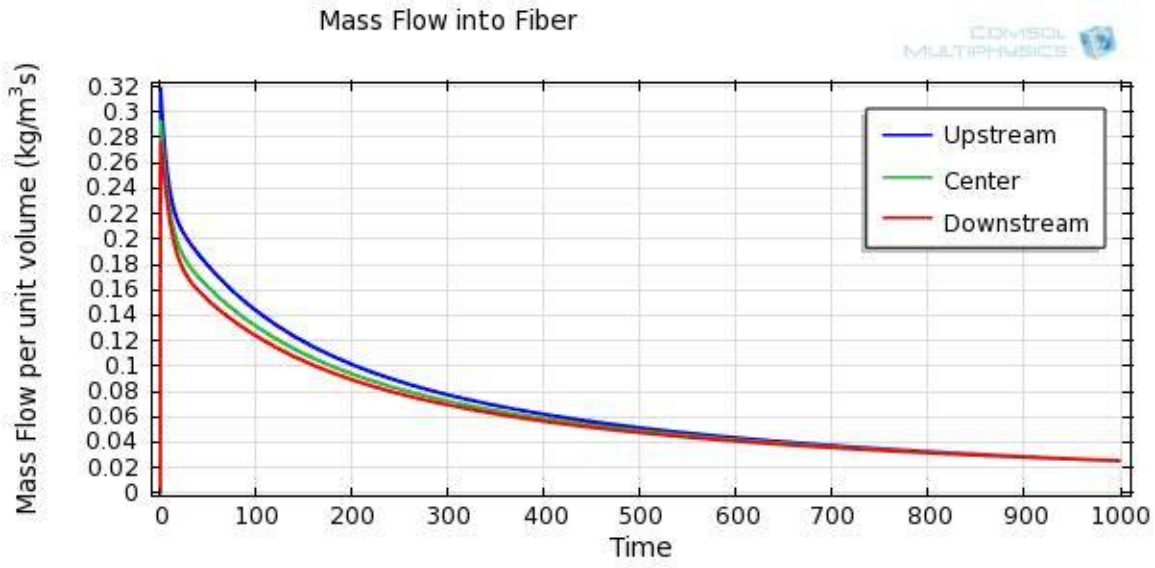

Figure 38. Mass flow into fibers

As discussed earlier, the permeability is humidity dependent. When the humidity increases the fibers absorb more moisture and swell accordingly. It's no surprise then that the permeability given in Figure 39 decreases as the humidity increases. To an extent, the vapor absorption makes the permeability non-homogeneous during transient states since the permeability changes downstream.

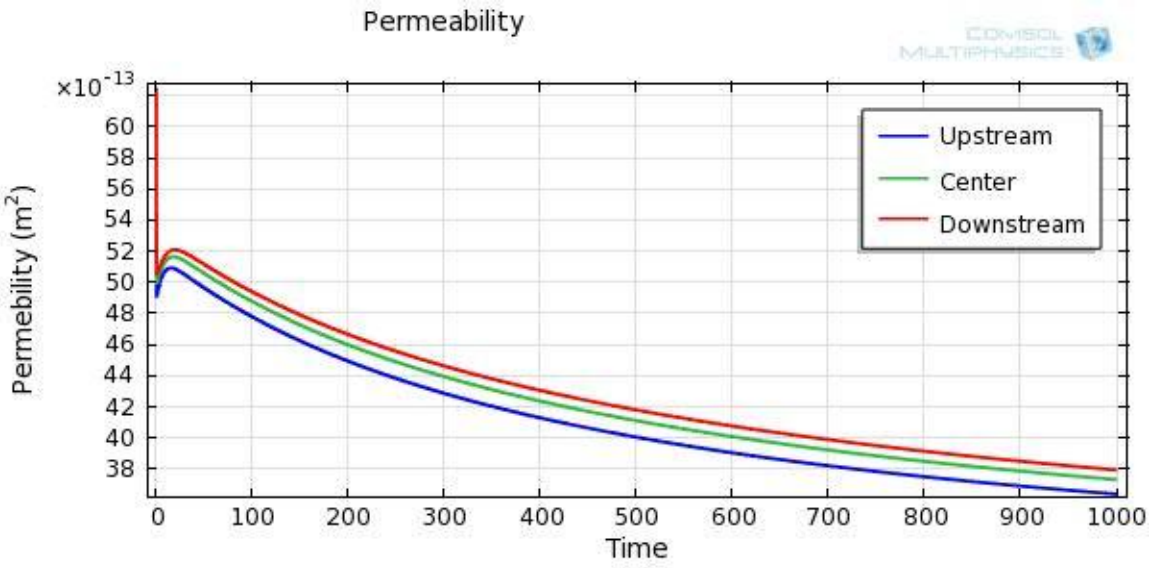

Figure 39. Permeability of PM

What hasn't been presented thus far is the temperature, which is provided in Figure 40. As can be seen, $T - T_{in}$ for both the present work and from the experiments of Gibson & Charmchi 1997(2) are similar. However, note that although the maximum temperatures are similar, the decay rate is not. It is believed that this is due to the simplified absorption equation used to model the mass flow in and out the fiber. It should also be

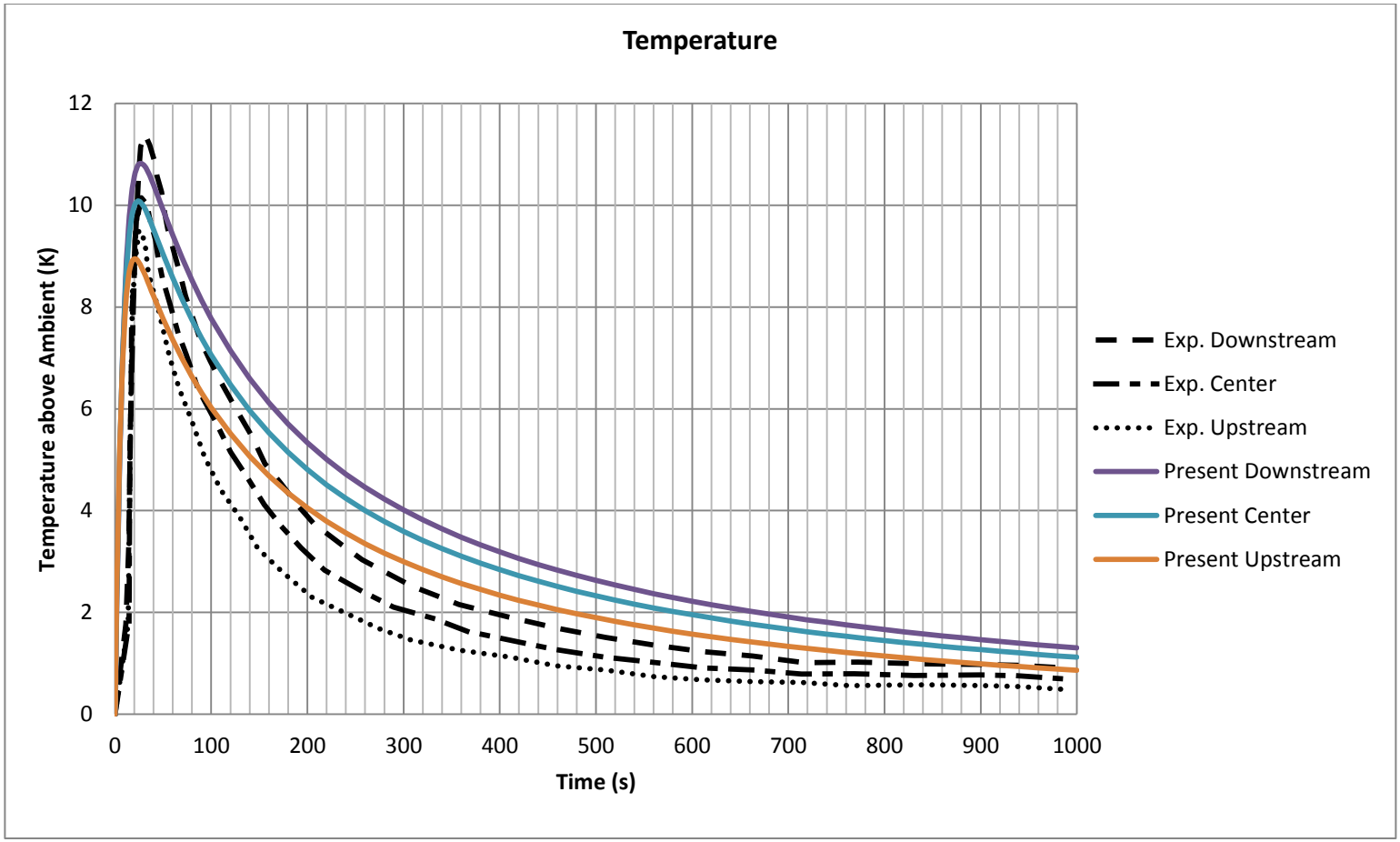

Figure 40. Temperature over time for present work and experimental

noted that the temperature spike is much larger than expected. In addition, the convection causes the temperature decay seen in the plot.

Having investigated the initial results for this case, we now turn our attention to the coupled nature of the physics modeled. As an example, with an increase in humidity, the water will be absorbed into the fiber, which will lead to a temperature rise and later a decrease in the humidity in the PM (from temperature rise and absorption). All this happens as the convective flow cools (in this case) the PM, which in turn increases the humidity. Thus, one can see that there is a balance of all the physics involved. The use of absorption can quickly complicate the problem, as the source terms vary.

Chapter 6

Conclusions

A multiphysics model was developed to study the aspects and properties of porous media that effect heat and mass transfer. The model made use of COMSOL's equation-based PDE interface to solve the equations for heat and mass transfer. Conjugate modeling is inherent in the equation-based approach. This allowed heat and mass transfer to be simultaneously accounted for in the porous material as well as outside the PM, where the convective transfer coefficients need not be known a priori. Hence, any porous material regardless of geometry or properties can be investigated.

Since the flow field can potentially have a strong influence on transport, flow over a cylinder in cross-flow was modeled to ensure that a time-accurate solution could be obtained using the equation-based approach, and that it compares well with experimental data. These two objectives were accomplished and it was found that the PDE formulation presents a solution that agrees well with experimental data as well as COMSOL's desktop physics interface. With the flow field solver established, attention was directed to the porous medium.

A simple diffusion problem was modeled for free fluid and porous media with a good agreement between the present work and experimental data. For the porous media simulations without the use of a tortuosity factor, the results were not as favorable. This only reinforced the need to model a tortuosity factor to account for the dispersion and molecule-pore interaction. Therefore, the volume averaging theory is

appropriate to define an effective diffusion coefficient, which can yield accurate results for gaseous diffusion in porous media.

Even when convection is added, as in the case of steady parallel flow, with zero normal flow through a PM, diffusion dominates the mass transfer process. It was found that when the flow is turned through the PM and a normal flow component exists (even if it is small in magnitude), the mass transfer inceases significantly. Different types of materials, namely hygroscopic and non-hygroscopic, were considered and it was shown that the convective heat and mass transfer through the PM depend on the permeability. Fiber swelling was found to greatly inhibit mass transfer since the pores are being "closed off". As a result, the permeability decreases which has the potential to make convection in the medium irrelevant. Thus, it was concluded that the more hygroscopic a material is the less heat and mass can be transported through it.

Transient effects for hygroscopic porous media give very interesting results. Most notable is the temperature rise (in this work) or temperature fall due to changes in the humidity. Although the humidity change modeled here was rather extreme compared to most physical situations, it was shown that water vapor absorption can have a significant effect on thermal comfort. Also, if the material absorbed "large" amounts of water vapor quickly – that is the sorption curve was steep and the fiber diffusion coefficient was high – higher fabric temperatures could be reached. Fiber properties, such as fiber diameter and fiber diffusion coefficient, thus have a significant impact on the transient behavior of the fabric. It must be noted that these transient

effects subside quickly, and therefore, the properties that effect long term thermal comfort are more important.

List of References

Bird, R. B., Stewart, W. E., & Lightfoot, E. N. (2002). *Transport Phenomena* (2nd ed.). New York: John Wiley & Sons.

Canuto, C., & Cimolin, F. (2011). A sweating model for the internal ventilation of a motorcycle helmet. *Computers and Fluids, 43*, 29-37.

Davarzani, H., Marcoux, M., Costeseque, P., & Quintard, M. (2010). Experimental measurement of the effective diffusion and thermodiffusion coefficients for binary gas mixture in porous media. *Chemical Engineering Science, 65*, 5092-5104.

De Bonis, M. V., & Ruocco, G. (2008). A generalized conjugate model for forced convection drying based on an evaporative kinetics. *Journal of Food Engineering, 89*, 232-240.

Defraeye, T. (2011). *Convective heat and mass transfer at exterior building surfaces.* Leuven: Katholieke Universiteit Leuven.

Defraeye, T., Blocken, B., & Carmeliet, J. (2012). Analysis of convective heat and mass transfer coefficients for convective drying of a porous flat plate by conjugate modeling. *International Journal of Heat and Mass Transfer, 55*, 112-124.

Defraeye, T., Blocken, B., Derome, D., Nicolai, B., & Carmeliet, J. (2012). Convective heat and mass transfer modeling at air-porous material interfaces: Overview of existing methods and relevance. *Chemical Engineering Science, 74*, 49-58.

Fan, J., Cheng, X., Wen, X., & Sun, W. (2004). An improved model of heat and moisture transfer with phase change and mobile condensates in fibrous insulation and comparison with experimental results. *International Journal of Heat and Mass Transfer, 47*, 2343-2352.

Fan, J., Luo, Z., & Li, Y. (2000). Heat and moisture transfer with sorption and condensation in porous clothing assemblies and numerical simulation. *International Journal of Heat and Mass Transfer, 43*, 2989-3000.

Gibson, P. W., & Charmchi, M. (1997). Coupled Heat and Mass Transfer Through Hygroscopic Porous Materials-Application to Clothing Layers. *53*(5), 183-194.

Gibson, P. W., & Charmchi, M. (1997). Modeling convection/diffusion processes in porous textiles with inclusion of humidity-dependent air permeability. *International Communications in Heat and Mass Transfer, 24*(5), 709-724.

Hang, X. D., Sun, W., & Ye, C. (2012). Finite volume solution of heat and moisture transfer through three-dimensional textile materials. *Computer and Fluids, 57*, 25-39.

Incropera, F. P., Dewitt, D. P., Bergman, T. L., & Lavine, A. S. (2007). *Fundamentals of Heat and Mass Transfer* (6th ed.). Hoboken, NJ: John Wiley & Sons. Inc.

Konig, M. U., & Eckelmann, H. (1998). A new Strouhal-Reynolds-number relationship for the circular cylinder in the range 47<Re<2e+05. *Physics of Fluids, 10*(7), 1547-1549.

Li, Y., & Zhu, Q. (2003). Simultaneous heat and moisture transfer with moisture sorption, condensation, and capillary liquid diffusion in porous textiles. *Textile Research Journal, 73*, 515-524.

Masmoudi, W., & Prat, M. (1991). Heat and mass transfer between a porous medium and a parallel external flow. Application to drying of capillary porous materials. *International Journal of Heat and Mass Transfer, 34*(8), 1975-1989.

Nield, D. A., & Bejan, A. (1999). *Convection in Porous Media* (2 ed.). New York: Springer-Verlag.

Progelhof, R. C., Throne, J. L., & Ruetsch, R. R. (1976). Methods for Prediciting the Thermal Conductivity of Composite Systems: A Review. *Polymer Engineering and Science, 16*(9), 615-625.

Prommas, R. (2011). Theoretical and experimental study of heat and mass transfer mechanism during convective drying of multi-layered porous packed bed. *International Communications in Heat and Mass Transfer, 38*, 900-905.

Rogers, J. A., & Kaviany, M. (1992). Funicular and evaporative-front regimes in convective drying of granular beds. *International Journal of Heat and Mass Transfer, 35*(2), 469-480.

Wehner, J. A., Miller, B., & Rebenfeld, L. (1987). Moisture Induced Changes in Fabric Structure as Evidence by Air Permeability Measurements. *Textile Research Journal, 57*, 247-256.

Whitaker, S. (1977). Simultaneous, Heat, Mass and Momentum Transfer in Porous Media: A Theory of Drying. *Advances in Heat Transfer, 13*, 119-203.

Zhang, Q., Li, B., & Sun, W. (2011). Heat and sweat transport through clothing assemblies with phase changes, condensation/evaporation and absorption. *Proceedings of the Royal Society A, 467*, 3469-3489.

Vita

Seth Pemberton was born in Nashville, TN, to the parents of Lynn and Keith Pemberton. He is the second of two children with older sister Ashley. He attended Una Elementary School, Cameron Middle School, JFK Middle School, and to Antioch High School. After graduation, he attended Tennessee Technological University where he decided to major in Mechanical Engineering. A year into the program he was persuaded by Dr. Sam Narimetla to also major in Mathematics. He obtained Bachelors of Science degrees in Mechanical Engineering and Mathematics from Tennessee Technological University in May of 2011. The following fall, he started graduate school at The University of Tennessee seeking a Masters degree in Thermal Fluid Science in Mechanical Engineering. He graduated with a Masters of Science degree in Mechanical Engineering in December 2013. He is continuing his education with a PhD in Mechanical Engineering at The University of Tennessee.